

# Proving periodic solutions and branches in the 2D Swift Hohenberg PDE with hexagonal and triangular symmetry

Dominic Blanco \*

February 16, 2026

## Abstract

In this article, we enforce space group symmetries in Fourier series to rigorously prove the existence of smooth, periodic solutions in partial differential equations (PDEs) with hexagonal and triangular symmetries. In particular, we provide the necessary analytical and numerical tools to construct Fourier series of functions on the hexagonal lattice. This allows one to build approximate solutions that are periodic. Moreover, to generate the periodic tiling, we can use one symmetric hexagon for  $D_6$  symmetry and two symmetric triangles for  $D_3$  symmetry. We derive a Newton-Kantorovich approach based on the construction of an approximate inverse around an approximate solution,  $\bar{u}$ . More specifically, we verify a condition based on the computation of explicit bounds. The strategy for constructing  $\bar{u}$ , the approximate inverse, and the computation of these bounds will be presented. We demonstrate our approach on the 2D Swift-Hohenberg PDE by proving the existence of  $D_3$  and  $D_6$  periodic solutions. We then perform proofs of branches of solutions by using Chebyshev series. The algorithmic details to perform the proof can be found on Github.

**Key words.** Periodic Solutions, Branches of Solutions, Swift Hohenberg, Hexagonal Lattice Symmetries, Dihedral symmetry, Computer-Assisted Proofs

## 1 Introduction

In this paper, we develop a methodology for constructively proving the existence (and local uniqueness) of solutions to partial differential equations (PDEs) with symmetries representable on the hexagonal lattice. More specifically, we will focus on  $D_3$  and  $D_6$ -symmetric solutions. By  $D_j$ , we mean the dihedral group of order  $2j$  which is the symmetry group of the  $j$ -gon. These groups have presentation

$$D_j = \langle r, s \mid r^n = s^2 = 1, rs = sr^{-1} \rangle.$$

We will illustrate such an approach in the case of the 2D Swift-Hohenberg (SH) PDE, for which we establish steady states with dihedral symmetries, namely

$$0 = (I_d + \nabla^2)^2 u + \mu u - \gamma u^2 + u^3, \quad u = u(x), \quad u \text{ is } u(x) = u(g \cdot x) \text{ for all } g \in D_j. \quad (1)$$

Note that we have set  $u_t = 0$  as we are looking for steady states. We wish to prove the existence, local uniqueness, and symmetry of solutions to (1). The Swift-Hohenberg PDE has been investigated in a wide variety of studies. In particular, (1) is known to exhibit a rich variety of well documented dihedral solutions. Various numerical and analytical studies of SH have led to a deeper understanding of dihedral patterns such as hexagonal [25, 26] and square [29] patterns. More generally, the works of [8], [21], and [22] demonstrate an approach to numerically compute dihedral solutions. By using radial coordinates, the authors provide a method to construct approximate solutions using a Galerkin projection starting with  $\mu$  small. By then performing continuation, one can obtain localized planar patterns of various dihedral symmetries. These can form both spot patterns (see

---

\*McGill University, Department of Mathematics and Statistics, 805 Sherbrooke Street West, Montreal, QC, H3A 0B9, Canada. [dominic.blanco@mail.mcgill.ca](mailto:dominic.blanco@mail.mcgill.ca)

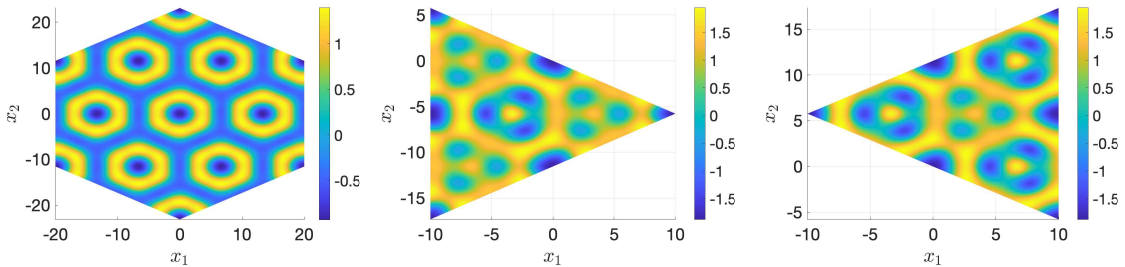


Figure 1: An approximate solution on the branch presented in Figure 12 (green point) when  $\mu \approx 0.01$  (L). An approximate solution on the branch presented in Figure 10 (green point) when  $\mu \approx -0.3$  on  $\Delta_1$  (C) and  $\Delta_2$  (R). See Theorem 2.2 for a definition.

[21]) and ring patterns (see [22]). Proofs in Swift-Hohenberg have been obtained before. For instance, under certain hypotheses, [1] obtains proofs of existence of some patterns. More generally several existence results for  $\mu$  small have been obtained in [1, 9, 24, 25, 26, 27, 28]. In particular, by using a bifurcation argument, a proof of existence of branches of patterns with  $\mu \in (0, \mu^*)$ , for some  $\mu^* > 0$  can be obtained. This argument relies on the implicit function theorem or various fixed-point theorems. Computer assisted proofs have also been used before in 2D and 3D to obtain existence results on rectangular domains in [19, 20]. This restriction on the value of  $\mu$  was removed by the authors of [34] provided that the solution is radially symmetric. In the aforementioned work, the authors present a method for rigorously proving radially symmetric solutions that does not depend on the value of  $\mu$ . Using the radially symmetric ansatz, the PDE is transformed into an ordinary differential equation. The approach then relies on a rigorous enclosure of the center stable manifold by using a Lyapunov-Perron operator. This allows one to solve a boundary value problem on  $(0, \infty)$ . This method does not provide restrictions on the value of  $\mu$ ; however, it is restricted to solutions with radial symmetry. This symmetry restriction was then removed by the authors of [15]. Indeed, the authors of the aforementioned work obtained rigorous proofs of three localized patterns in (1) that are not radially symmetric without as many restrictions on  $\mu$ . The approach is based on that of [14], which provides a construction method based on Fourier series for rigorously computing steady states on  $\mathbb{R}^m$ . The only requirement made in [15] is that  $\mu > 0$  so that the linear part of the equation is invertible. This is a necessary assumption when attempting to prove localized patterns using the approach developed by the authors of [14]. Additionally, the authors were able to construct  $D_2$  symmetric solutions using invariant functions under reflections about the  $x$  and  $y$  axis. The method was then extended further in [6]. A general method for proving any symmetry of a localized pattern was developed. To begin, the authors construct  $u_0$  with as much symmetry as possible. Then, the authors build a new approximate solution, denoted  $w_0$ , which is the average of  $u_0$  when acted on by the elements of the desired symmetry group  $\mathcal{G}$ . As  $w_0$  now has the desired symmetry, the authors demonstrate a constructive approach to prove the existence of a symmetric solution to the PDE. This approach works as long as the symmetry enforced in  $u_0$  can be represented on the square lattice. The authors remark that symmetries on the hexagonal lattice can be proven, but they were unable to take advantage of this in the computational approach.

In this paper, we demonstrate how we can use symmetries on the hexagonal lattice for proving the existence of periodic solutions to (1). As there is still a heavy interest in periodic solutions to (1), we would like to provide a general approach to prove the symmetry for any value of  $\mu$ . Note that we will be able to prove solutions when  $\mu < 0$  as we are interested in periodic solutions, and our approach will not require the linear part to be invertible. To begin, we will need a way to represent symmetries on the hexagonal lattice in Fourier series. A posteriori approaches for rigorously verifying the symmetry of solutions obtained via computer-assisted proofs have been developed. These techniques are applicable to a wide variety of symmetries, but have the restriction in that they do not reduce the number of Fourier coefficients required. As our problems will be posed in 2D, performing proofs without any reduction would be difficult if not impossible. With this in mind, we are interested in techniques which reduce the computational complexity when a symmetry is present. Such techniques on symmetric Fourier coefficients have been deeply developed

in [30] and [31]. More specifically, the authors describe a way to build a Fourier series that possesses the desired symmetry. The methods developed in [30] and [31] are applicable to any space group in any dimension. The authors use an algorithm to compute a reduced set of Fourier indices under the symmetry of a space group. Furthermore, the method allows one to determine the specific relations amongst the coefficients. In particular, it relies on computing a set which contains one element from each orbit (see [18] for a definition) of the given space group. Such a set is called a fundamental domain, denoted  $\mathcal{Z}_{\text{dom}}(\mathcal{G})$ . To demonstrate the use of  $\mathcal{Z}_{\text{dom}}(\mathcal{G})$ , suppose  $u$  is a Fourier series with Fourier coefficients  $(u_n)_{n \in \mathbb{Z}^m}$ . If an index,  $n$ , is in the fundamental domain, then the other elements in its orbit (in the sense of group action) will have the same value. That is, for any  $g \in \mathcal{G}$ ,  $u_n = u_{g \cdot n}$  where  $\cdot$  denotes the group action. This relation already reduces the number of Fourier indices one must store. This is especially important when performing computer assisted proofs in higher dimensions, such as in [33]. Additionally, the authors of [30] and [31] define two additional sets. The first set,  $\mathcal{Z}_{\text{triv}}(\mathcal{G})$ , is called the trivial set. This set contains all Fourier indices which have values of 0. The indices which are 0 depend on the symmetry being enforced. The second is defined as

$$\mathcal{Z}_{\text{sym}}(\mathcal{G}) \stackrel{\text{def}}{=} \mathbb{Z}^m \setminus \mathcal{Z}_{\text{triv}}(\mathcal{G}).$$

Since the trivial set contains all indices corresponding to coefficients which are 0, the second set,  $\mathcal{Z}_{\text{sym}}(\mathcal{G})$ , contains all indices corresponding to coefficients which are non-zero. Hence, we would like to disregard the indices in  $\mathcal{Z}_{\text{triv}}$  numerically and only consider those in  $\mathcal{Z}_{\text{sym}}$ . Once  $\mathcal{Z}_{\text{dom}}(\mathcal{G})$  and  $\mathcal{Z}_{\text{sym}}(\mathcal{G})$  are obtained, one can define the reduced set of Fourier coefficients

$$\mathcal{Z}_{\text{red}}(\mathcal{G}) \stackrel{\text{def}}{=} \mathcal{Z}_{\text{dom}}(\mathcal{G}) \cap \mathcal{Z}_{\text{sym}}(\mathcal{G}). \quad (2)$$

Indeed, the relations determined by  $\mathcal{Z}_{\text{dom}}(\mathcal{G})$  and  $\mathcal{Z}_{\text{triv}}(\mathcal{G})$  allow one to write a Fourier series only featuring indices in  $\mathcal{Z}_{\text{red}}(\mathcal{G})$ . Such a Fourier series will enforce the needed relations numerically. This allows one to build an approximate solution that is necessarily of the symmetry enforced. Using this approach in [30], the authors obtain rigorous proofs of existence and local uniqueness of periodic solutions to 3D Ohta-Kawasaki with a SG229 and SG230 symmetry. In [31], they generalize the approach and allow for one to attempt rigorous proofs for any space group symmetry. Since the rigorous approach used relies on a contraction argument, it can be shown that the true solution also has the symmetry of the approximate solution. The method was also applied in [33], where symmetries on the range of the function were also considered. The same algorithm can be applied and the computational details are outlined in Sections 5 and 6 of the aforementioned paper.

In this paper, we will focus on  $D_3$  and  $D_6$  symmetry, which are both expressible on the hexagonal lattice. This means we will need to provide the necessary estimates to perform a computer-assisted proof (CAP) using Fourier series posed on the hexagonal lattice. As the methods developed by the authors of [30, 31] are done generally for any space group on the square or hexagonal lattice, their techniques readily apply. However, we would like to use `RadiiPolynomial.jl` in Julia [23] to perform our rigorous computations. This means we need to develop the Julia code to enforce  $D_3$  and  $D_6$  symmetries. Indeed, [23] only has the ability to enforce  $D_2$ -symmetry. One can also enforce  $D_4$ -symmetry by using the code provided at [3]. We wish to generalize the code of [3] to provide a complete package of all dihedral space groups. The implementation of such a package is nontrivial in a variety of aspects. Firstly, one must compute the reduced set of Fourier indices and store it in a vector. This means we need to find a mapping between the entries of a vector and the reduced set of indices which are tuples since we are in 2D. Following this, we need to develop a way to produce the necessary objects for our CAP. This includes addition, convolution, ways to build multiplication operators, ways to evaluate the sequence with this symmetry, norms, and more. We describe these in more detail in Section 3.2.1. Moreover, since we have  $D_3$  and  $D_6$ -symmetry, we would like to demonstrate how we can generate the periodic tiling on  $\mathbb{R}^2$  using triangles and hexagons respectively. This is of interest as Fourier series on the hexagonal lattice will be defined on a parallelogram; however, under the symmetry of  $D_3$  and  $D_6$ , we will show that one can use two  $D_3$ -symmetric triangles to create the  $D_3$  tiling and one  $D_6$ -symmetric hexagon for the  $D_6$  tiling. This is possible since triangles and hexagons form a tiling of the plane.

The rest of this paper is organized as follows. In Section 2, we begin with a discussion on symmetric Fourier series on the hexagonal lattice. This will allow us to enforce  $D_3$  and  $D_6$  symmetries

theoretically. Then, we discuss how one can generate the periodic tiling via triangles and hexagons. As it turns out, the result is fundamentally different for triangles and hexagons, so our discussion will require two proofs: one for  $D_3$  (see Theorem 2.2) and one for  $D_6$  (see Theorem 2.3). Following this in Section 3, we perform our computer-assisted analysis to prove  $D_3$  and  $D_6$  periodic solutions. This begins with a discussion of the numerical aspects in Section 3.2. We include more details on the implementation of the  $D_3$  and  $D_6$  symmetries in a way that is compatible with the library [23] in Section 3.2.1. Then we obtain the required bounds to perform the CAP in Section 3.3, followed by a presentation of our results in Section 3.4. In Section 4, we develop the necessary tools for proving branches of solutions with  $D_3$  and  $D_6$ -symmetry. This not only provides us with a proof of the branch, but also that the entire branch is symmetric. That is, each periodic pattern on this branch can be generated by either two triangles (in the case of  $D_3$ ) or one hexagon (in the case of  $D_6$ ). The results are presented in Section 4.3. Finally, we conclude in Section 5, and remark on future directions.

## 2 Symmetric Fourier coefficients

As mentioned in the introduction, our approach heavily relies on symmetric Fourier series. From that perspective, we introduce related notations and results from [30] and [31]. To begin, let  $D_j$  be the dihedral group of order  $2j$ . We will focus on  $j = 3, 6$  as we are interested in solutions that are periodic on a triangle and/or hexagon. Suppose our function has period  $2d$  where  $0 < d < \infty$ . Then, we define

$$\tilde{n} = (\tilde{n}_1, \tilde{n}_2) \stackrel{\text{def}}{=} \left( \frac{n_1\pi}{d}, \frac{n_2\pi}{d} \right) \in \mathbb{R}^2$$

for all  $(n_1, n_2) \in \mathbb{Z}^2$ . We want to restrict to Fourier series representing  $D_j$ -symmetric functions for  $j = 3, 6$ . To do so, we present the following lemma.

**Lemma 2.1.** *Let  $u$  be a Fourier series of the form*

$$u(x) = \sum_{n \in \mathbb{Z}^2} u_n e^{i(\mathcal{L}\tilde{n}) \cdot x}$$

where  $\mathcal{L} \stackrel{\text{def}}{=} \begin{bmatrix} 1 & -\frac{1}{2} \\ 0 & \frac{\sqrt{3}}{2} \end{bmatrix}$  is the change of basis for the hexagonal lattice. Let  $D_j$  be the dihedral group of order  $2j$ . Therefore, each  $g \in D_j$  has a unitary representation of the form

$$gx = \mathcal{A}x + b$$

where  $\mathcal{A} \in M_{2 \times 2}(\mathbb{R})$  and  $b \in [0, 1]^2$ . Next, define

$$\beta_g(n) \stackrel{\text{def}}{=} \mathcal{L}^{-1} \mathcal{A} \mathcal{L} n, \quad \alpha_g(n) \stackrel{\text{def}}{=} \exp(2\pi i \beta_g(n) \cdot b).$$

Then, it follows that  $u(x) = u(gx)$  for all  $g \in D_j$  and  $x \in \mathbb{R}^2$  if and only if  $\alpha_g(n) u_{\beta_g(n)} = u_n$ . In this case, we say that  $u$  has a  $D_j$ -Fourier series representation.

*Proof.* The proof can be found in [31]. □

Note that the domain of periodicity for  $u$  when it is of the form (3) is

$$\square_0 \stackrel{\text{def}}{=} \mathcal{L}^{-T}(-d, d)^2 = \left\{ (x_1, x_2) \text{ such that } \frac{x_1}{\sqrt{3}} - \frac{2}{\sqrt{3}}d \leq x_2 \leq \frac{x_1}{\sqrt{3}} + \frac{2}{\sqrt{3}}d, -d \leq x_1 \leq d \right\}.$$

Lemma 2.1 provides a correspondence between symmetry of functions and symmetry of the coefficients. This lemma also has an immediate corollary.

**Corollary 2.1.** *Let  $u$  be a  $D_j$ -Fourier series where  $D_j$  is the dihedral group of order  $2j$ . Let  $\text{orb}_{D_j}(n)$  be the orbit of  $n \in \mathbb{Z}^2$  in  $\mathcal{G}$  (cf. [18]). We define the orbit as*

$$\text{orb}_{D_j}(n) = \{g \cdot n, \text{ for all } g \in D_j\}.$$

Let  $\mathcal{Z}_{\text{red}}(D_j)$  be defined as in (2). Then, the  $D_j$ -Fourier series of  $u$  can be written with indices in  $\mathcal{Z}_{\text{red}}(D_j)$ . More specifically,

$$u(x) = \sum_{n \in \mathcal{Z}_{\text{red}}(D_j)} u_n \sum_{k \in \text{orb}_{D_j}(n)} e^{i\mathcal{L}\bar{k} \cdot x}. \quad (3)$$

*Proof.* The proof can be found in [31].  $\square$

Essentially,  $\mathcal{Z}_{\text{red}}(D_j)$  contains all coefficients necessary to compute a  $D_j$ -Fourier series. In the case of dihedral groups, this set is a strict subset of  $\mathbb{Z}^2$ . Therefore, we restrict the indexing of  $D_j$ -symmetric functions to  $\mathcal{Z}_{\text{red}}(D_j)$  and construct the full series by symmetry if needed. Let us now discuss how we can obtain tilings of the plane with  $D_3$  and  $D_6$ -symmetry.

## 2.1 Periodic tilings with Hexagons and Triangles

As we are attempting to prove periodic solutions with  $D_3$  and  $D_6$  symmetry, we are interested in demonstrating how to construct a periodic tiling using triangles and hexagons respectively. That is, the  $D_j$  periodic pattern can be described via some  $D_j$ -symmetric domain(s). Let us begin by stating the result for  $D_3$ .

**Theorem 2.2.** *Let  $u$  be a periodic function with domain of periodicity  $\square_0$  satisfying  $D_3$ -symmetry. Let  $\Delta_1, \Delta_2$  be two equilateral triangular domains*

$$\begin{aligned} \Delta_1 &\stackrel{\text{def}}{=} \left\{ (x_1, x_2) \text{ such that } -\frac{x_1}{\sqrt{3}} \leq x_2 \leq \frac{x_1}{\sqrt{3}} + \frac{3}{\sqrt{3}}d, -2d \leq x_1 \leq 2d \right\} \\ \Delta_2 &\stackrel{\text{def}}{=} \left\{ (x_1, x_2) \text{ such that } \frac{x_1}{\sqrt{3}} - \frac{4}{\sqrt{3}}d \leq x_2 \leq -\frac{x_1}{\sqrt{3}}, -2d \leq x_1 \leq 2d \right\}. \end{aligned}$$

Then,  $u|_{\Delta_k}$  for  $k = 1, 2$  is  $D_3$ -symmetric about the centroid of  $\Delta_k$ , and the periodic pattern can be generated by translations of  $\Delta_1$  and  $\Delta_2$ .

*Proof.* Similar to  $\square_0$ , we introduce

$$\square_{2d} \stackrel{\text{def}}{=} \left\{ (x_1, x_2) \text{ such that } \frac{x_1}{\sqrt{3}} - \frac{4}{\sqrt{3}}d \leq x_2 \leq \frac{x_1}{\sqrt{3}} + \frac{4}{\sqrt{3}}d, -2d \leq x_1 \leq 2d \right\}. \quad (4)$$

Note that  $\square_{2d} \stackrel{\text{def}}{=} \mathcal{L}^{-T}(-2d, 2d)^2$  is also a domain of periodicity, albeit not the minimal one. We will show that  $\square_{2d}$  can be divided into two equilateral triangles, which are  $\Delta_1$  and  $\Delta_2$ . To do so, we must prove that the opposite angles of  $\square_{2d}$  measure  $60^\circ$  and  $120^\circ$ . Its vertices are

$$\begin{aligned} V_1 &\stackrel{\text{def}}{=} \mathcal{L}^{-T} \begin{bmatrix} 2d \\ 2d \end{bmatrix} = \begin{bmatrix} 2d \\ 2\sqrt{3}d \end{bmatrix}, \quad V_2 \stackrel{\text{def}}{=} \mathcal{L}^{-T} \begin{bmatrix} 2d \\ -2d \end{bmatrix} = \begin{bmatrix} 2d \\ -\frac{2}{\sqrt{3}}d \end{bmatrix}, \\ V_3 &\stackrel{\text{def}}{=} \mathcal{L}^{-T} \begin{bmatrix} -2d \\ 2d \end{bmatrix} = \begin{bmatrix} -2d \\ \frac{2}{\sqrt{3}}d \end{bmatrix}, \quad V_4 \stackrel{\text{def}}{=} \mathcal{L}^{-T} \begin{bmatrix} -2d \\ -2d \end{bmatrix} = \begin{bmatrix} -2d \\ -2\sqrt{3}d \end{bmatrix}. \end{aligned}$$

We will now find the angle at the vertex  $V_1$ . To do so, we will form two vectors, denoted  $\vec{v}_1$  and  $\vec{v}_2$  that go through this vertex.

$$\vec{v}_1 \stackrel{\text{def}}{=} V_1 - V_2 = \begin{bmatrix} 2d - 2d \\ 2\sqrt{3}d - (-\frac{2}{\sqrt{3}}d) \end{bmatrix} = \begin{bmatrix} 0 \\ \frac{8}{\sqrt{3}}d \end{bmatrix}, \quad \vec{v}_2 \stackrel{\text{def}}{=} V_1 - V_3 = \begin{bmatrix} 2d - (-2d) \\ 2\sqrt{3}d - \frac{2}{\sqrt{3}}d \end{bmatrix} = \begin{bmatrix} 4d \\ \frac{4}{\sqrt{3}}d \end{bmatrix}.$$

Now, notice that

$$\vec{v}_1 \cdot \vec{v}_2 = \frac{32}{3}d^2, \quad |\vec{v}_1| = \frac{8}{\sqrt{3}}d, \quad |\vec{v}_2| = \frac{8}{\sqrt{3}}d.$$

Hence, we obtain

$$\theta = \arccos\left(\frac{\frac{32}{3}d^2}{\frac{8}{\sqrt{3}}d \cdot \frac{8}{\sqrt{3}}d}\right) = \arccos\left(\frac{1}{2}\right) = 60^\circ.$$

This shows that one of the interior angles of  $\square_{2d}$  is  $60^\circ$ , meaning the non-opposite angle is  $120^\circ$ . This means we can split this parallelogram into two equilateral triangles.

Let us now show that the two equilateral triangles we obtain are  $\Delta_1$  and  $\Delta_2$ . By our previous computation, we know that the angles at the vertices  $V_2$  and  $V_3$  are  $120^\circ$  angles. Hence, the two equilateral triangles can be found by drawing a line between  $V_2$  and  $V_3$ . This line has a slope of

$$\frac{-\frac{2}{\sqrt{3}}d - \frac{2}{\sqrt{3}}d}{2d - -2d} = \frac{-\frac{4}{\sqrt{3}}d}{2d + 2d} = \frac{\frac{4}{\sqrt{3}}d}{4d} = -\frac{1}{\sqrt{3}}.$$

With the slope computed, the line we want is given by

$$\begin{aligned} x_2 + \frac{2}{\sqrt{3}}d &= -\frac{1}{\sqrt{3}}(x_1 - 2d) \\ x_2 + \frac{2}{\sqrt{3}}d &= -\frac{1}{\sqrt{3}}x_1 + \frac{2}{\sqrt{3}}d \\ x_2 &= -\frac{1}{\sqrt{3}}x_1. \end{aligned}$$

Then, according to the definition of  $\square_{2d}$  given in (4), it is clear that we obtain  $\Delta_1$  and  $\Delta_2$ . Since triangles tile the plane, and we have a periodic function, we can create a tiling using  $\Delta_1$  and  $\Delta_2$ .

Now that we have obtained that  $\Delta_1$  and  $\Delta_2$  can tile the plane, we need to show that  $u$  is  $D_3$ -symmetric on  $\Delta_k$  for  $k = 1, 2$ . The centroids of  $\Delta_1$  and  $\Delta_2$ ,  $c_1$  and  $c_2$  respectively, are

$$c_1 \stackrel{\text{def}}{=} \left(\frac{2d}{3}, \frac{2d}{\sqrt{3}}\right), \quad c_2 \stackrel{\text{def}}{=} \left(-\frac{2d}{3}, -\frac{2d}{\sqrt{3}}\right).$$

To proceed generally, we introduce  $c \stackrel{\text{def}}{=} \left(\pm\frac{2d}{3}, \pm\frac{2d}{\sqrt{3}}\right)$ . We must now show that  $u$  is invariant under  $D_3$ -symmetry operations done about  $c$ . Let  $g \cdot x = \mathcal{A}x$  for some  $g \in D_3$  and  $\mathcal{A} \in M_{2 \times 2}(\mathbb{R})$ . Then,

$$u(\mathcal{A}(x - c) + c) = u(\mathcal{A}(x - c + \mathcal{A}^{-1}c)) = u(\mathcal{A}(x + (\mathcal{A}^{-1} - I_d)c)) = u(x + (\mathcal{A}^{-1} - I_d)c)$$

where the last step followed from the fact that  $u$  is  $D_3$ -symmetric. If  $\mathcal{A} = \begin{bmatrix} 1 & 0 \\ 0 & -1 \end{bmatrix}$ , then

$$u(x + (\mathcal{A}^{-1} - I_d)c) = u\left(x \mp \begin{bmatrix} 0 \\ \frac{4d}{\sqrt{3}} \end{bmatrix}\right) = u(x)$$

where the last step followed from the fact that  $\mathcal{L}^T \begin{bmatrix} 0 \\ \mp\frac{4d}{\sqrt{3}} \end{bmatrix} = \mp 2d$ . Hence, we can disregard it by periodicity of  $\square_0$ . Note that we require the periodicity on  $\square_0$  here despite using  $\square_{2d}$  to define  $\Delta_k$  for  $k = 1, 2$ . Let  $R_\theta$  be the rotation matrix by  $\theta$ . If  $\mathcal{A} = R_{\frac{2\pi}{3}}$  is a rotation, then

$$u(x + (\mathcal{A}^{-1} - I_d)c) = u\left(x + \begin{bmatrix} 0 \\ \mp\frac{4\sqrt{3}d}{3} \end{bmatrix}\right) = u(x)$$

which we can again disregard by periodicity on  $\square_0$ . Showing that the result holds for other group elements of  $D_3$  will use similar steps. This concludes the proof.  $\square$

We present the analogous result for  $D_6$ .

**Theorem 2.3.** *Let  $u$  be a periodic function satisfying  $D_6$ -symmetry. Let*

$$\square_1 \stackrel{\text{def}}{=} \left\{ \left( x_1 - d, x_2 + \frac{d}{\sqrt{3}} \right) \mid (x_1, x_2) \in \square_0 \right\}, \square_2 \stackrel{\text{def}}{=} \left\{ R_{\frac{2\pi}{3}} x \text{ for all } x \in \square_1 \right\}, \square_3 \stackrel{\text{def}}{=} \left\{ R_{\frac{4\pi}{3}} x \text{ for all } x \in \square_1 \right\}$$

where  $R_\theta$  is the rotation matrix by  $\theta$ . Let  $\circ_0 \stackrel{\text{def}}{=} \square_1 \cup \square_2 \cup \square_3$ . Then,  $u$  satisfies periodic boundary conditions on  $\circ_0$ .

*Proof.* We first shift  $\square_0$  to  $\square_1$ , which is still a domain of periodicity by definition. Now, since  $u$  is  $D_6$ -symmetric, we are able to perform both a  $120^\circ$  and  $240^\circ$  rotation about  $(0, 0)$  and preserve the function values. That is,  $u|_{\square_k}$  for  $k = 1, 2, 3$  are equivalent under  $D_6$ -symmetry operations. Then, if we define  $\circ_0 \stackrel{\text{def}}{=} \square_1 \cup \square_2 \cup \square_3$ , we will obtain a regular hexagonal domain. Moreover, since  $u$  is  $D_6$ -symmetric, it follows that  $u|_{\circ_0}$  is invariant under  $D_6$ -symmetry operations. Since hexagons tile the plane, we can generate the periodic pattern of  $u$  using copies of  $\circ_0$ . Hence, we have proven that  $u$  is periodic on  $\circ_0$ .  $\square$

**Remark 2.1.** *The previous two theorems both provide results on tiling the plane using triangles and hexagons; however, the result for  $D_3$  differs from that of  $D_6$ . In the case of  $D_3$ , we have that  $u|_{\Delta_1} \neq u|_{\Delta_2}$ . This is due to the fact that  $D_3$ -symmetry does not contain the needed element to relate  $\Delta_1$  and  $\Delta_2$ . In other words,  $\Delta_1$  and  $\Delta_2$  generate distinct sublattices of the hexagonal lattice which, when repeated periodically by translation, can generate the  $D_3$  pattern. On the other hand, in the case of  $D_6$ , we only need to consider  $\circ_0$  where  $u|_{\circ_0}$  does respect all the  $D_6$ -symmetry operations. As a result,  $\circ_0$  is a domain of periodicity on its own, providing us with a periodic function on a hexagon. To summarize, for  $D_3$ , we define two distinct equilateral triangles, each of which respect the  $D_3$ -symmetry. When tiled together, these two triangles can generate the full  $D_3$  periodic pattern. For  $D_6$ , we define one hexagon which respects the  $D_6$ -symmetry. This hexagon on its own can be considered a domain of periodicity, meaning we have a periodic function on a hexagon. In fact, when the symmetry is  $D_6$ , one can show that  $u|_{\Delta_1} = u|_{\Delta_2}$ , which is another way to generate the hexagonal tiling.*

Now that we have obtained the desired results for tiling the plane using triangles and hexagons when the function has  $D_3$  or  $D_6$ -symmetry respectively, let us begin our computer assisted analysis.

### 3 Computer Assisted Analysis

In this section, we will discuss the computer assisted aspects of our approach. From now on, we will refer to  $u$  as a sequence rather than a function unless other specified. First, we introduce some notation. Let  $\ell_{j,\nu}^1$  denote the following Banach space

$$\ell_{j,\nu}^1 \stackrel{\text{def}}{=} \left\{ u = (u_n)_{n \in \mathcal{Z}_{\text{red}}(D_j)} : \|u\|_1 \stackrel{\text{def}}{=} \sum_{n \in \mathcal{Z}_{\text{red}}(D_j)} \alpha_n |u_n| \nu^n < \infty \right\}, \text{ where } (\alpha_n)_{n \in \mathcal{Z}_{\text{red}}(D_j)} \stackrel{\text{def}}{=} |\text{orb}_{D_j}(n)|.$$

Note that  $\ell_{j,\nu}^1$  possesses the same sequences as the usual  $\ell_\nu^1$  for sequences indexed on  $\mathcal{Z}_{\text{red}}(D_j)$ . Given Fourier coefficients  $u = (u_n)_{n \in \mathbb{Z}^2}, v = (v_n)_{n \in \mathbb{Z}^2}$  corresponding to the usual exponential Fourier series expansion, we define the discrete convolution as

$$(u * v)_n = \sum_{k \in \mathbb{Z}^2} u_{n-k} \text{conj}(v)_k$$

where  $\text{conj}(\cdot)$  denotes complex conjugation. In the case of symmetric sequences  $\ell_{j,\nu}^1$ , we still denote  $u * v$  the discrete convolution representing the product of two functions for consistency. Additionally, given  $u \in \ell_{j,\nu}^1$ , we define

$$\begin{aligned} \mathfrak{u} : \ell_{j,\nu}^1 &\rightarrow \ell_{j,\nu}^1 \\ v &\mapsto u * v \end{aligned}$$

the discrete convolution operator associated to  $u$ . To begin, we will state the main theorem we wish to apply. Following this, we will construct various quantities needed to apply this theorem. Then, we will estimate the needed bounds which we will then rigorously evaluate on the computer. Let us begin with the main theorem.

### 3.1 Newton-Kantorovich Approach

As we are considering the 2D Swift Hohenberg PDE, we write

$$f(u) = Lu + G(u), \quad L \stackrel{\text{def}}{=} (I_d + \nabla^2)^2 + \mu I_d, \quad G(u) \stackrel{\text{def}}{=} -\gamma u^2 + u^3. \quad (5)$$

Let  $S$  be a Banach space corresponding to the image of  $f$  under  $\ell_{j,\nu}^1$ . That is,  $f : \ell_{j,\nu}^1 \rightarrow S$ . Suppose we have  $\bar{u} \in \ell_{j,\nu}^1$  an approximate solution to (5). That is,  $f(\bar{u}) \approx 0$ . Then, we state the following theorem.

**Theorem 3.1.** *Let  $A^\dagger \in \mathcal{B}(\ell_{j,\nu}^1, S)$ . Also let  $A \in \mathcal{B}(S, \ell_{j,\nu}^1)$  be injective. Moreover, let  $Y_0, Z_0, Z_1$  be non-negative constants, and let  $Z_2(r) : (0, \infty) \rightarrow [0, \infty)$  be a non-negative function such that*

$$\begin{aligned} \|Af(\bar{u})\|_{1,\nu} &\leq Y_0 \\ \|I_d - AA^\dagger\|_{\mathcal{B}(\ell_{j,\nu}^1)} &\leq Z_0 \\ \|A(Df(\bar{u}) - A^\dagger)\|_{\mathcal{B}(\ell_{j,\nu}^1)} &\leq Z_1 \\ \|A(Df(u) - Df(\bar{u}))\|_{\mathcal{B}(\ell_{j,\nu}^1)} &\leq Z_2(r)\|u - \bar{u}\|_{1,\nu} \text{ for all } u \in B_r(\bar{u}). \end{aligned}$$

If there exists  $r > 0$  such that

$$\frac{1}{2}Z_2(r)r^2 - (1 - Z_0 - Z_1)r + Y_0 < 0, \text{ and } Z_1 + Z_0 + Z_2(r)r < 1$$

then there exists a unique  $\tilde{u} \in \overline{B_r(\bar{u})} \subset \ell_{j,\nu}^1$  such that  $f(\tilde{u}) = 0$ , where  $B_r(\bar{u})$  is the open ball of  $\ell_{j,\nu}^1$  centered at  $\bar{u}$  with radius  $r$ .

*Proof.* The proof can be found in [33]. □

**Remark 3.1.** *Note that  $f : \ell_{j,\nu}^1 \rightarrow S$  and we did not specify  $S$  beyond the fact that it is the image of  $f$  under  $\ell_{j,\nu}^1$ . We emphasize that this is not problematic as  $S$  typically does not play a role in the application of Theorem 3.1. As a result, we do not specify  $S$ .*

### 3.2 Numerical Aspects

In this section, we will discuss the numerical aspects of our approach. We first introduce some notation. Define

$$I^N \stackrel{\text{def}}{=} \{n \in \mathcal{Z}_{\text{red}}(D_j), |n_1| \leq N, |n_2| \leq N\}.$$

Let  $v = (v_n)_{n \in \mathcal{Z}_{\text{red}}(D_j)}$

$$(\pi^N v)_n \stackrel{\text{def}}{=} \begin{cases} v_n & n \in I^N \\ 0 & \text{else} \end{cases}, \quad (\pi_N v)_n \stackrel{\text{def}}{=} \begin{cases} 0 & n \in I^N \\ v_n & \text{else} \end{cases}.$$

To obtain a numerical approximation of the solution on  $\square_0$ , we relied on a naive approach. We would first choose the number of Fourier coefficients  $N$ . Next, randomly generate a grid of points of the corresponding size,  $2N + 1 \times 2N + 1$ . We think of this random grid as representing a random function, denoted  $\bar{U}_2$ . We then computed a Fourier series approximation of the function  $\bar{U}_2$ . That is, we compute  $(\bar{a}_n)_{n \in \mathbb{Z}^2}$  such that

$$\bar{U}_1(x) \stackrel{\text{def}}{=} \sum_{n \in \mathbb{Z}^2} \bar{a}_n e^{i\mathcal{L}\bar{n} \cdot x}$$



and we should have  $\bar{U}_2 \approx \bar{U}_1$ . At this step, we do not expect the coefficients  $\bar{a}_n$  to satisfy the symmetry relation for  $D_j$ . Indeed, since  $\bar{U}_2$  was a randomly chosen function, it has no reason to be  $D_j$ -symmetric and hence neither does its Fourier series approximation  $\bar{U}_1$ . As we are only interested in  $D_j$ -symmetric solutions for this paper, we would simply choose one element from each orbit, and define

$$\bar{U}_0(x) \stackrel{\text{def}}{=} \sum_{n \in \mathcal{Z}_{\text{red}}(D_j)} \bar{a}_n \sum_{k \in \text{orb}_{D_j}(n)} e^{i\mathcal{L}\bar{k} \cdot x}. \quad (6)$$

Note that the choice of element from each orbit is not important to us as we are building a random initial guess. From here, we run a Newton method on  $\bar{U}_0$  to refine our initial guess. More often than not, Newton's method would diverge as our guess was random and not particularly close to a solution. After a sufficient amount of attempts, our Newton method would converge. We denote the result of the convergence  $\bar{u} \stackrel{\text{def}}{=} (\bar{u}_n)_{n \in \mathcal{Z}_{\text{red}}(D_j)}$  and use it as our approximate solution for the proof. Our approach is not guaranteed to work for any PDE and solution; however, it was sufficient for our purposes as we managed to find multiple candidates where Newton converged.

Let us now construct  $A$  and  $A^\dagger$ . These choices will consist of two parts: a finite part which can be represented as a matrix, and an infinite part which we will control.  $A^\dagger$  will be an approximation of  $Df(\bar{u})$ . That is, for a given  $h \in \ell_{j,\nu}^1$ , we define

$$(A^\dagger h)_n \stackrel{\text{def}}{=} \begin{cases} [\pi^N Df(\bar{u})\pi^N h]_n & n \in I^N \\ ((1 + |\mathcal{L}\tilde{n}|^2)^2 + \mu)h_n & n \in \mathbb{Z}^2 \setminus I^N \end{cases}.$$

Notice that for  $n \in I^N$ , we consider the action of  $\pi^N Df(\bar{u})\pi^N$  on  $h$ . This operator can be represented as a finite matrix. We then only consider the action of the linear part in the tail. This leads us to a natural way to define  $A$ , which is suppose to be an approximate inverse for  $Df(\bar{u})$ . In particular, we choose

$$A^N \approx (\pi^N Df(\bar{u})\pi^N)^{-1}.$$

As mentioned before, the operator  $A^N$  can be represented a matrix, which can be stored on the computer. This is the finite part of  $A$ . For the tail, rather than considering the full  $Df(\bar{u})^{-1}$ , we only choose the inverse of the linear part,  $L$ . This leads us to define

$$(Ah)_n \stackrel{\text{def}}{=} \begin{cases} (A^N \pi^N h)_n & n \in I^N \\ \frac{h_n}{(1 + |\mathcal{L}\tilde{n}|^2)^2 + \mu} & n \in \mathbb{Z}^2 \setminus I^N \end{cases}.$$

With this definition, observe that

$$\|\pi^N A\|_{\mathcal{B}(\ell_{j,\nu}^1)} \leq \max_{n \in \mathbb{Z}^2 \setminus I^N} \frac{1}{|(1 + |\mathcal{L}\tilde{n}|^2)^2 + \mu|} \stackrel{\text{def}}{=} \frac{1}{L_N}.$$

where

$$L_N \stackrel{\text{def}}{=} \min_{n \in \mathbb{Z}^2 \setminus I^N} |(1 + |\mathcal{L}\tilde{n}|^2)^2 + \mu| \quad (7)$$

We will frequently use this bound in our computations to follow. With  $\bar{u}$ ,  $A^\dagger$ , and  $A$  now detailed in construction, let us describe how we enforce the  $D_3$  and  $D_6$  symmetry in these objects.

### 3.2.1 Enforcing $D_3$ and $D_6$ symmetries in Fourier series

Our approach relies on a the ability to construct functions of the form (3) and rigorous numerics. To do so, we rely primarily on two Julia packages. The first is IntervalArithmetic.jl, [2]. This package allows us to perform computations on intervals, which makes our results rigorous. The second is RadianPolynomial.jl, [23]. This package is designed with many useful tools for computer assisted proofs. One of its main tools is the ability to store vectors as "sequence structures." By a sequence

structure, we mean a vector that corresponds to a sequence of Fourier coefficients. By storing our data in its corresponding sequence structure, we are able to rely on a variety of operations built into [23]. In particular, this package allows us to perform addition, subtraction, convolutions, build multiplication operators, build linear operators, compute norms, take derivatives, etc. One can do this provided that the sequence structure with the desired symmetry they wish to prove exists in [23]. This is not the case for this project. In fact, [23] only allows one to enforce up to  $D_2$  symmetry. For dihedral groups, this limitation was partially addressed by one of the authors of [13]. Indeed, one of the authors developed a code for  $D_4$ -symmetric sequences. This sequence structure was then used to perform the proofs of Theorems 6.1, 6.2, 6.3, and 6.4 in Section 6 of [13]. The code is available at [3] and is fully compatible with [23].

Since we require sequence structures for  $D_3$  and  $D_6$  symmetry, we extended the work done in [3] to include  $D_3$  and  $D_6$  sequence structures. The result, which we will call `dihedral.jl` can be found on Github at [5]. This code can be viewed as an add-on to [23]. More specifically, the sequence structures implemented in [5] are fully compatible with the tools of [23]. Our contribution was to create the sequence structures for the dihedral symmetries and define the operations necessary to perform operations such as addition, subtraction, convolution, build multiplication operators, build linear operators, compute norms, etc. One of the challenges we would like to emphasize is that we needed to find a way to store the reduced sets,  $\mathcal{Z}_{\text{red}}(D_j)$  for  $j = 3, 6$ . As mentioned earlier, a sequence structure is a vector whose entries represent the indices of a sequence with a specific symmetry. Therefore, the first challenge is to find a mapping between the entries of a vector and the indices of a sequence. Mathematically speaking, we are required to find a mapping from  $\mathcal{Z}_{\text{red}}(D_j) \rightarrow \mathbb{N}$ . In general, this task is non-trivial as such a mapping is not guaranteed to exist. By studying  $\mathcal{Z}_{\text{red}}(D_j)$  for  $j = 3, 6$ , we were eventually able to find a mappings which worked. The details can be found in [5]. Additionally, the sets  $I^{\mathcal{N}}$  for  $D_3$  and  $D_6$  do not completely fill the indices of  $\mathbb{Z}^2$ . For example,  $(5, 1) \in \text{orb}_{D_6}((4, -1))$ . Therefore, in order to include  $(4, -1)$ , we must also include  $(5, 1)$ . That means that  $(4, -1) \notin I^4$ , and one must set the index  $(4, -1)$  to 0. The reason is due to the definition of  $I^{\mathcal{N}}$  in 3.2, which states that we must only includes indices whose entries are less than  $\mathcal{N}$  in absolute value. This leads to some numerical complications. More specifically, it turns out that the orbits of the entries of  $I^{\mathcal{N}}$  for  $D_3$  and  $D_6$  only contain every index for  $|n_1|, |n_2| \leq \frac{\mathcal{N}}{2}$ . This means that a  $D_3$  or  $D_6$  Fourier series of size  $\mathcal{N}$  can be viewed as a Fourier series of order  $\frac{\mathcal{N}}{2}$  plus a few more indices up to order  $\mathcal{N}$ . In practice, this makes proofs which use these symmetries require additional runtime than those done with symmetries expressed on the square lattice. The primary culprit of the slow runtime is convolution since those are performed by unfolding the sequence. When one unfolds this sequence to perform convolution, it will numerically behave as though it is a sequence of size  $\mathcal{N}$  despite the number of 0 indices in this set. The benefits still outweigh this problem as we can not only enforce the symmetry, but the proofs take less memory since matrices are smaller with less coefficients.

With the sequence structures at [5] available, we can indeed restrict the indices to  $\mathcal{Z}_{\text{red}}(D_j)$  and define  $\bar{u}_0$  as in (6). Once we run Newton on  $\bar{u}_0$  to obtain  $\bar{u}$ , we can evaluate  $\pi^{\mathcal{N}} Df(\bar{u}) \pi^{\mathcal{N}}$  on the computer. Once we have this matrix available, we can invert it, and obtain our approximate inverse  $A^{\mathcal{N}}$  under the  $D_j$ -symmetry. With these objects now constructed numerically, we are ready to compute the bounds of Theorem 3.1. This will be the focus of the next section.

### 3.3 Computing the Bounds

We will now compute the bounds  $Y_0, Z_0, Z_1$ , and  $Z_2$ . Let us begin with  $Y_0$  and  $Z_0$ .

**Lemma 3.2.** *Let  $L_{N,K}$  be defined as in (7). Let  $Y_0, Z_0 > 0$  be defined as*

$$Y_0 \stackrel{\text{def}}{=} \|A^{\mathcal{N}} f(\bar{u})\|_{1,\nu} + \frac{1}{L_N} \|(\pi^{3\mathcal{N}} - \pi^{\mathcal{N}})G(\bar{u})\|_{1,\nu}, \quad Z_0 \stackrel{\text{def}}{=} \|\pi^{\mathcal{N}} - A^{\mathcal{N}} \pi^{\mathcal{N}} Df(\bar{u}) \pi^{\mathcal{N}}\|_{\mathcal{B}(\ell_{j,\nu}^1)}.$$

*Then, it follows that  $\|Af(\bar{u})\|_{1,\nu} \leq Y_0$  and  $\|I_d - AA^\dagger\|_{\mathcal{B}(\ell_{j,\nu}^1)} = Z_0$ .*

*Proof.* For  $Y_0$ , we start from the definition.

$$\begin{aligned} \|Af(\bar{u})\|_{1,\nu} &= \|\pi^N Af(\bar{u})\|_{1,\nu} + \|\pi_N Af(\bar{u})\|_{1,\nu} = \|A^N f(\bar{u})\|_{1,\nu} + \|\pi_N AG(\bar{u})\|_{1,\nu} \\ &\leq \|A^N f(\bar{u})\|_{1,\nu} + \|\pi_N A\|_{\mathcal{B}(\ell_{j,\nu}^1)} \|\pi_N G(\bar{u})\|_{1,\nu} \\ &\leq \|A^N f(\bar{u})\|_{1,\nu} + \frac{1}{L_N} \|(\pi^{3N} - \pi^N)G(\bar{u})\|_{1,\nu} \end{aligned}$$

as desired. For  $Z_0$ , notice that since the tail of  $A$  and  $A^\dagger$  cancel exactly, we are left with the finite part. Hence, the equality is immediate.  $\square$

Next, we examine the  $Z_2$  bound. We state its lemma.

**Lemma 3.3.** *Let  $q \stackrel{\text{def}}{=} (q_n)_{n \in \mathcal{Z}_{\text{red}}(D_j)} = (-2\gamma\delta_n + 6\bar{u}_n)_{n \in \mathcal{Z}_{\text{red}}(D_j)}$  where  $\bar{u} = (\bar{u}_n)_{n \in \mathcal{Z}_{\text{red}}(D_j)}$  and  $\delta_n$  is the Kronecker delta. Let  $L_N$  be defined as in (7). Now, let  $Z_2(r) : (0, \infty) \rightarrow [0, \infty)$  be defined as*

$$Z_2(r) \stackrel{\text{def}}{=} \left( \|A^N\|_{\mathcal{B}(\ell_{j,\nu}^1)} + \frac{1}{L_N} \right) (\|q\|_{1,\nu} + 3r).$$

Then,  $\|A(Df(u) - Df(\bar{u}))\|_{\mathcal{B}(\ell_{j,\nu}^1)} \leq Z_2(r)r$ .

*Proof.* To begin, observe that

$$\begin{aligned} \|A(Df(u) - Df(\bar{u}))\|_{\mathcal{B}(\ell_{j,\nu}^1)} &= \|A(DG(u) - DG(\bar{u}))\|_{\mathcal{B}(\ell_{j,\nu}^1)} \leq \|A\|_{\mathcal{B}(\ell_{j,\nu}^1)} \|DG(u) - DG(\bar{u})\|_{\mathcal{B}(\ell_{j,\nu}^1)} \\ &\leq \left( \|A^N\|_{\mathcal{B}(\ell_{j,\nu}^1)} + \frac{1}{L_N} \right) \|DG(u) - DG(\bar{u})\|_{\mathcal{B}(\ell_{j,\nu}^1)}. \end{aligned} \quad (8)$$

Now, since  $u \in B_r(\bar{u})$ , there exists a  $v \in B_r(0)$  such that  $u = \bar{u} + v$ . Note that  $\|v\|_{1,\nu} \leq r$ . Also let  $h \in \ell_{j,\nu}^1$  such that  $\|h\|_{1,\nu} \leq 1$ . Then, we compute

$$\begin{aligned} (DG(u) - DG(\bar{u}))h &= (DG(\bar{u} + v) - DG(\bar{u}))h = (-2\gamma(\bar{u} + v) + 3(\bar{u} + v)^2 + 2\gamma\bar{u} - 3\bar{u}^2)h \\ &= ((-2\gamma I_d + 6\bar{u})v + 3v^2)h \\ &= (qv + 3v^2)h. \end{aligned}$$

Using this, we obtain

$$\|DG(u) - DG(\bar{u})\|_{\mathcal{B}(\ell_{j,\nu}^1)} \leq \|qv + 3v^2\|_{1,\nu} \leq \|q\|_{1,\nu} \|v\|_{1,\nu} + 3\|v\|_{1,\nu}^2 \leq \|q\|_{1,\nu} r + 3r^2$$

where we used that  $\ell_{j,\nu}^1$  (see 3) is a Banach algebra. Using this in (8) yields the result.  $\square$

**Remark 3.2.** *The computation of  $Z_2$  was done primarily in the interest of computational intensity. Indeed, step (8) is not a particularly sharp estimate. We did so in order to simplify the estimates done on the computer and increase the speed of the code. This is of higher interest in Section 4, where the runtime becomes an issue.*

Before we compute the  $Z_1$  bound, we define  $\bar{v} \stackrel{\text{def}}{=} (\bar{v}_n)_{n \in \mathcal{Z}_{\text{red}}(D_j)} = (-2\gamma\bar{u}_n + 3(\bar{u} * \bar{u})_n)_{n \in \mathcal{Z}_{\text{red}}(D_j)}$ . Notice that by definition, we have  $\bar{v} = \pi^{2N}\bar{v}$ . We will now state the lemma for  $Z_1$ .

**Lemma 3.4.** *Recall that  $\bar{v} \stackrel{\text{def}}{=} \pi^{2N}\bar{v}$  and hence  $\bar{v}_n \neq 0$  for all  $n \in I^{2N}$ . Let  $\bar{V} = (\bar{V}_n)_{n \in \mathcal{Z}_{\text{red}}(D_j)}$ ,  $\phi = (\phi_n)_{n \in \mathcal{Z}_{\text{red}}(D_j)} \in \ell_{j,\nu}^1$  where*

$$\bar{V}_n \stackrel{\text{def}}{=} \begin{cases} 0 & n = (0, 0) \\ \bar{v}_n & n \in I^{2N} \setminus \{(0, 0)\} \end{cases}, \quad \phi_n \stackrel{\text{def}}{=} \begin{cases} \frac{\|\bar{V}\|_\infty}{\nu^{N+1}} & n \in I^N \\ 0 & \text{else} \end{cases}.$$

Let  $Z_1 > 0$  be defined as

$$Z_1 \stackrel{\text{def}}{=} \|A^N \phi\|_{1,\nu} + \frac{1}{L_N} \|\bar{v}\|_{1,\nu}.$$

Then, it follows that  $\|A(Df(\bar{u}) - A^\dagger)\|_{\mathcal{B}(\ell_{j,\nu}^1)} \leq Z_1$ .

*Proof.* To begin, given  $h \in \ell_{j,\nu}^1$ ,  $\|h\|_{1,\nu} \leq 1$ , let

$$z \stackrel{\text{def}}{=} (Df(\bar{u}) - A^\dagger)h.$$

Then, observe that we can write

$$\|A(Df(\bar{u}) - A^\dagger)\|_{\mathcal{B}(\ell_{j,\nu}^1)} = \|A(Df(\bar{u}) - A^\dagger)h\|_{1,\nu} = \|Az\|_{1,\nu} = \|A^N z\|_{1,\nu} + \|\pi_N Az\|_{1,\nu}. \quad (9)$$

We now have two terms in (9) to bound. For the first term, notice that for  $n \in I^N$  we can write

$$(\pi^N z)_n = \sum_{m \in \mathbb{Z}^2} \bar{v}_{n-m} \text{conj}(h)_n - \sum_{m \in I^N} \bar{v}_{n-m} \text{conj}(h)_n = \sum_{m \in \mathbb{Z}^2 \setminus I^N} \bar{v}_{n-m} \text{conj}(h)_n = (\bar{v} * \pi_N h)_n$$

Now, we claim that  $|(\bar{v} * \pi_N h)_n| \leq \phi_n$  for all  $n \in I^N$ . First, let  $W_1(n) \subset \mathbb{Z}^2$  be the set of  $m$  for which  $\bar{v}_{n-m} \neq 0$ . Also let  $W_2 \stackrel{\text{def}}{=} \mathbb{Z}^2 \setminus I^N$ , which is the set of  $m$  for which  $\pi_N h \neq 0$ . Then, observe that

$$\begin{aligned} |(\bar{v} * \pi_N h)_n| &\leq \left| \sum_{m \in \mathbb{Z}^2} \bar{v}_{n-m} (\pi_N \text{conj}(h))_m \right| \leq \sum_{m \in W_1(n) \cap W_2} \left( \frac{|\bar{v}_{n-m}|}{\nu^{|m|}} \right) |h_m| \nu^{|m|} \\ &\leq \sum_{m \in W_1(n) \cap W_2} \left( \sup_{k \in W_1(n) \cap W_2} \frac{|\bar{v}_{n-k}|}{\nu^{|k|}} \right) |h_m| \nu^{|m|} \\ &\leq \sup_{m \in W_1(n) \cap W_2} \frac{|\bar{v}_{n-m}|}{\nu^{|m|}} \|h\|_{1,\nu}. \end{aligned} \quad (10)$$

Since  $v_k = 0$  whenever  $k \in \mathbb{Z}^2 \setminus I^{2N}$  and we only need  $n \in I^N$ , we obtain the overestimate that  $W_1(n) \subset I^{3N}$ . Additionally, since  $(\pi_N h)_n = 0$  for all  $n \in I^N$ , we get

$$|(\bar{v} * \pi_N h)_n| \leq \max_{m \in I^{3N} \setminus I^N} \frac{|\bar{v}_{n-m}|}{\nu^{|m|}} \leq \frac{1}{\nu^{N+1}} \max_{m \in I^{3N} \setminus I^N} |\bar{v}_{n-m}| \leq \frac{1}{\nu^{N+1}} \max_{k \in I^N, m \in I^{3N} \setminus I^N} |\bar{v}_{k-m}|. \quad (11)$$

Now, since  $I^N$  and  $I^{3N} \setminus I^N$  are disjoint, the index of  $(0, 0)$  is never attained when computing the maximum in (11). As a result, we can write

$$\max_{k \in I^N, m \in I^{3N} \setminus I^N} |\bar{v}_{k-m}| = \max_{k \in I^N, m \in I^{3N} \setminus I^N} |\bar{V}_{k-m}| = \|\bar{V}\|_\infty.$$

Hence, we indeed see that  $|(\bar{v} * \pi_N h)_n| \leq \phi_n$  for all  $n \in I^N$ . This means we can say

$$\|A^N z\|_{1,\nu} = \|A^N (\bar{v} * \pi_N h)\|_{1,\nu} \leq \|A^N \phi\|_{1,\nu}. \quad (12)$$

Finally, we examine the second term of (9).

$$\|\pi_N Az\|_{1,\nu} \leq \|\pi_N A\|_{\mathcal{B}(\ell_{j,\nu}^1)} \|\pi_N z\|_{1,\nu} \leq \frac{1}{L_N} \|z\|_{1,\nu} \leq \frac{1}{L_N} \|\bar{v}\|_{1,\nu} \|h\|_{1,\nu} \leq \frac{1}{L_N} \|\bar{v}\|_{1,\nu} \quad (13)$$

where we used the Banach algebra property and the fact that  $\|h\|_{1,\nu} \leq 1$ . Therefore, we can combine (12) and (13) to get

$$\|A(Df(\bar{u}) - A^\dagger)\|_{\mathcal{B}(\ell_{j,\nu}^1)} \leq \|A^N \phi\|_{1,\nu} + \frac{1}{L_N} \|\bar{v}\|_{1,\nu} \stackrel{\text{def}}{=} Z_1$$

as desired.  $\square$

**Remark 3.3.** *The steps to estimate (12) were similar to those used by the authors of [7]. Indeed, if we had stopped at (10), we would have had the equivalent result for our problem. We decided to go further and introduce  $\bar{V}$  so we could obtain a uniform estimate for all  $n$ . This will be of interest in Section 4 where the uniform estimate is less computationally intensive for the estimates done on the computer.*

With the bounds now computed, we can present our results.

### 3.4 Results

In this section, we prove the existence of various periodic solutions with  $D_3$ -symmetry and  $D_6$ -symmetry. We construct our solution  $\bar{u} \in \ell_{j\nu}^1$  on the parallelogram  $\square_0$ . By using Theorems 2.2 and 2.3, we obtain that the corresponding function's periodic tiling can be generated by  $\Delta_1$  and  $\Delta_2$  in the case of  $D_3$ , and  $\circ_0$  for the case of  $D_6$ . We present these results along with a demonstration of the periodicity.

**Theorem 3.5 (The First Triangular Solution).** *Let  $\mu = 0.01, \gamma = 1.6$ . Moreover, let  $r_0 \stackrel{\text{def}}{=} 3 \times 10^{-5}$ . Then there exists a unique solution  $\tilde{u}$  to (5) in  $\overline{B_{r_0}(\bar{u})} \subset \ell_{3,1.15}^1$  and we have that  $\|\tilde{u} - u_0\|_{\ell_{3,1.15}^1} \leq r_0$ . Moreover, the periodic pattern  $\tilde{u}$  can be generated by a tiling of  $\Delta_1$  and  $\Delta_2$ .*

*Proof.* Choose  $N = 70, d = 10$ . Then, we perform the full construction described in Section 3.2 to build  $\bar{u}$  and  $A^N$ . Using [4, 5], we choose  $r_0 \stackrel{\text{def}}{=} 3 \times 10^{-5}$  and obtain

$$\|A^N\|_{\mathcal{B}(\ell_{3,1.15}^1)} \leq 150.21, Y_0 \stackrel{\text{def}}{=} 9.64 \times 10^{-6}, Z_2(r_0) \stackrel{\text{def}}{=} 25886.81, Z_1 \stackrel{\text{def}}{=} 0.175, Z_0 \stackrel{\text{def}}{=} 2.042 \times 10^{-9}.$$

We prove that these values satisfy Theorem 3.1. □

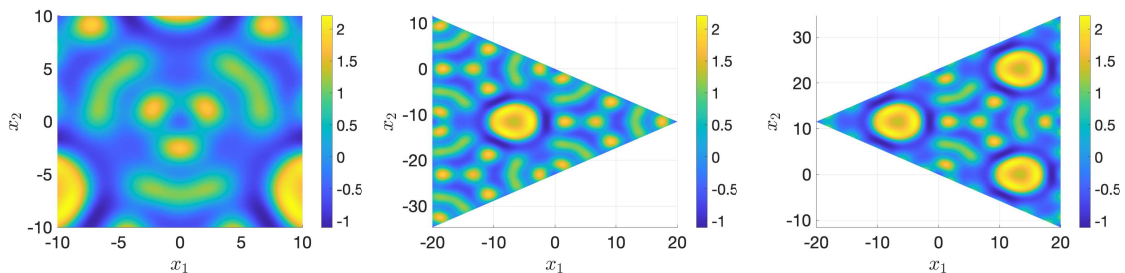


Figure 2: Plot of  $\bar{u}$  of an approximation of a  $D_3$  Pattern on  $(-10, 10)^2$  (L), the same approximation on  $\Delta_1$  (C), and the same approximation on  $\Delta_2$  (R).

**Theorem 3.6 (The Second Triangular Solution).** *Let  $\mu = 0.01, \gamma = 1.6$ . Moreover, let  $r_0 \stackrel{\text{def}}{=} 2 \times 10^{-4}$ . Then there exists a unique solution  $\tilde{u}$  to (5) in  $\overline{B_{r_0}(\bar{u})} \subset \ell_{3,1.38}^1$  and we have that  $\|\tilde{u} - u_0\|_{\ell_{3,1.38}^1} \leq r_0$ . Moreover, the periodic pattern  $\tilde{u}$  can be generated by a tiling of  $\Delta_1$  and  $\Delta_2$ .*

*Proof.* Choose  $N = 12, d = 5$ . Then, we perform the full construction described in Section 3.2 to build  $\bar{u}$  and  $A^N$ . Using [4, 5], we choose  $r_0 \stackrel{\text{def}}{=} 2 \times 10^{-4}$  and obtain

$$\|A^N\|_{\mathcal{B}(\ell_{3,1.38}^1)} \leq 44.06, Y_0 \stackrel{\text{def}}{=} 6.29 \times 10^{-6}, Z_2(r_0) \stackrel{\text{def}}{=} 923.91, Z_1 \stackrel{\text{def}}{=} 0.5788, Z_0 \stackrel{\text{def}}{=} 1.465 \times 10^{-12}.$$

We prove that these values satisfy Theorem 3.1. □

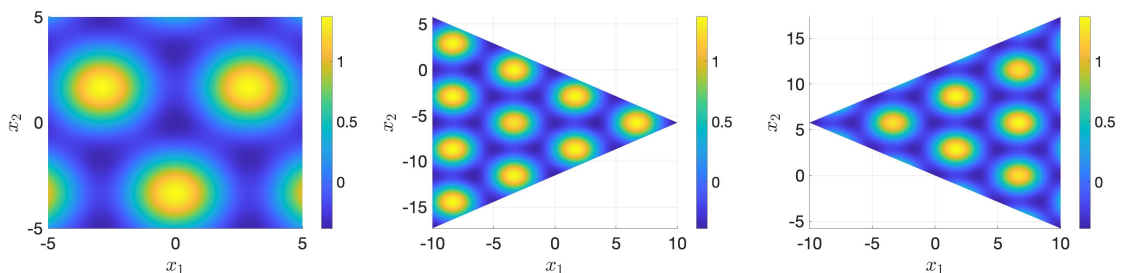


Figure 3: Plot of  $\bar{u}$  of an approximation of a  $D_3$  Pattern on  $(-5, 5)^2$  (L), the same approximation on  $\Delta_1$  (C), and the same approximation on  $\Delta_2$  (R).

**Theorem 3.7 (The Third Triangular Solution).** Let  $\mu = -0.01, \gamma = 1.7$ . Moreover, let  $r_0 \stackrel{\text{def}}{=} 2 \times 10^{-4}$ . Then there exists a unique solution  $\tilde{u}$  to (5) in  $\overline{B_{r_0}(\bar{u})} \subset \ell_{3,1.34}^1$  and we have that  $\|\tilde{u} - u_0\|_{\ell_{3,1.34}^1} \leq r_0$ . Moreover, the periodic pattern  $\tilde{u}$  can be generated by a tiling of  $\Delta_1$  and  $\Delta_2$ .

*Proof.* Choose  $N = 22, d = 5$ . Then, we perform the full construction described in Section 3.2 to build  $\bar{u}$  and  $A^N$ . Using [4, 5], we choose  $r_0 \stackrel{\text{def}}{=} 2 \times 10^{-4}$  and obtain

$$\|A^N\|_{\mathcal{B}(\ell_{3,1.34}^1)} \leq 13.616, Y_0 \stackrel{\text{def}}{=} 3.645 \times 10^{-5}, Z_2(r_0) \stackrel{\text{def}}{=} 447.7, Z_1 \stackrel{\text{def}}{=} 0.765, Z_0 \stackrel{\text{def}}{=} 1.377 \times 10^{-12}.$$

We prove that these values satisfy Theorem 3.1.  $\square$

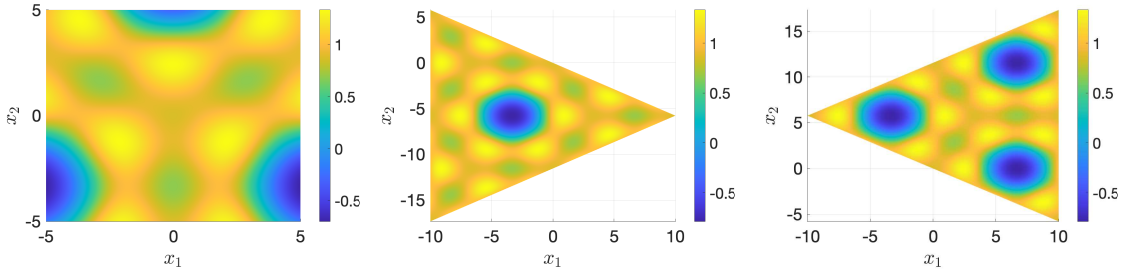


Figure 4: Plot of  $\bar{u}$  of an approximation of a  $D_3$  Pattern on  $(-5, 5)^2$  (L), the same approximation on  $\Delta_1$  (C), and the same approximation on  $\Delta_2$  (R).

**Theorem 3.8 (The Fourth Triangular Solution).** Let  $\mu = -0.2, \gamma = 2$ . Moreover, let  $r_0 \stackrel{\text{def}}{=} 9 \times 10^{-4}$ . Then there exists a unique solution  $\tilde{u}$  to (5) in  $\overline{B_{r_0}(\bar{u})} \subset \ell_{3,1.33}^1$  and we have that  $\|\tilde{u} - u_0\|_{\ell_{3,1.33}^1} \leq r_0$ . Moreover, the periodic pattern  $\tilde{u}$  can be generated by a tiling of  $\Delta_1$  and  $\Delta_2$ .

*Proof.* Choose  $N = 10, d = 5$ . Then, we perform the full construction described in Section 3.2 to build  $\bar{u}$  and  $A^N$ . Using [4, 5], we choose  $r_0 \stackrel{\text{def}}{=} 9 \times 10^{-4}$  and obtain

$$\|A^N\|_{\mathcal{B}(\ell_{3,1.33}^1)} \leq 11.935, Y_0 \stackrel{\text{def}}{=} 1.74 \times 10^{-4}, Z_2(r_0) \stackrel{\text{def}}{=} 255.3, Z_1 \stackrel{\text{def}}{=} 0.6921, Z_0 \stackrel{\text{def}}{=} 8.961 \times 10^{-13}.$$

We prove that these values satisfy Theorem 3.1.  $\square$

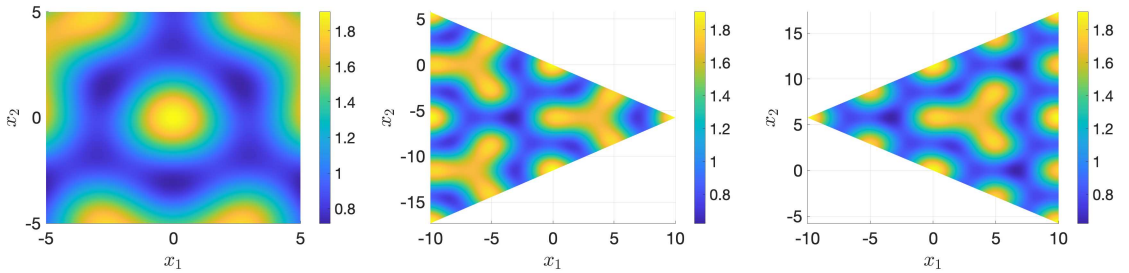


Figure 5: Plot of  $\bar{u}$  of an approximation of a  $D_3$  Pattern on  $(-5, 5)^2$  (L), the same approximation on  $\Delta_1$  (C), and the same approximation on  $\Delta_2$  (R).

**Theorem 3.9 (The First Hexagonal Solution).** Let  $\mu = -0.01, \gamma = 1.6$ . Moreover, let  $r_0 \stackrel{\text{def}}{=} 6 \times 10^{-3}$ . Then there exists a unique solution  $\tilde{u}$  to (5) in  $\overline{B_{r_0}(\bar{u})} \subset \ell_{6,1.3}^1$  and we have that  $\|\tilde{u} - u_0\|_{\ell_{6,1.3}^1} \leq r_0$ . Moreover,  $\tilde{u}$  is periodic on  $\mathcal{O}_0$ .

*Proof.* Choose  $N = 30, d = 10$ . Then, we perform the full construction described in Section 3.2 to build  $\bar{u}$  and  $A^N$ . Using [4, 5], we choose  $r_0 \stackrel{\text{def}}{=} 6 \times 10^{-3}$  and obtain

$$\|A^N\|_{\mathcal{B}(\ell_{6,1.3}^1)} \leq 15.577, Y_0 \stackrel{\text{def}}{=} 2.013 \times 10^{-4}, Z_2(r_0) \stackrel{\text{def}}{=} 632.8281, Z_1 \stackrel{\text{def}}{=} 0.4509, Z_0 \stackrel{\text{def}}{=} 6.485 \times 10^{-12}.$$

We prove that these values satisfy Theorem 3.1. □

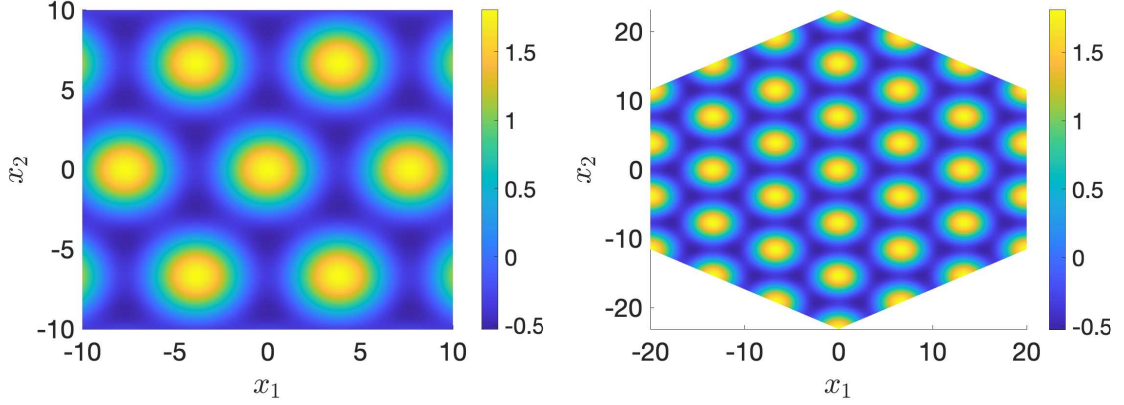


Figure 6: Plot of  $\bar{u}$  of an approximation of a  $D_6$  Pattern on  $(-10, 10)^2$  (L) and on  $\mathcal{O}_0$  (R).

**Theorem 3.10 (The Second Hexagonal Solution).** *Let  $\mu = -0.1, \gamma = 2$ . Moreover, let  $r_0 \stackrel{\text{def}}{=} 3 \times 10^{-5}$ . Then there exists a unique solution  $\tilde{u}$  to (5) in  $\overline{B_{r_0}(\bar{u})} \subset \ell_{6,1.37}^1$  and we have that  $\|\tilde{u} - u_0\|_{\mathcal{B}(\ell_{6,1.37}^1)} \leq r_0$ . Moreover,  $\tilde{u}$  is periodic on  $\mathcal{O}_0$ .*

*Proof.* Choose  $N = 26, d = 10$ . Then, we perform the full construction described in Section 3.2 to build  $\bar{u}$  and  $A^N$ . Using [4, 5], we choose  $r_0 \stackrel{\text{def}}{=} 3 \times 10^{-5}$  and obtain

$$\|A^N\|_{\mathcal{B}(\ell_{6,1.37}^1)} \leq 732.4, Y_0 \stackrel{\text{def}}{=} 4.27 \times 10^{-6}, Z_2(r_0) \stackrel{\text{def}}{=} 8766.03, Z_1 \stackrel{\text{def}}{=} 0.56031, Z_0 \stackrel{\text{def}}{=} 1.248 \times 10^{-10}.$$

We prove that these values satisfy Theorem 3.1. □

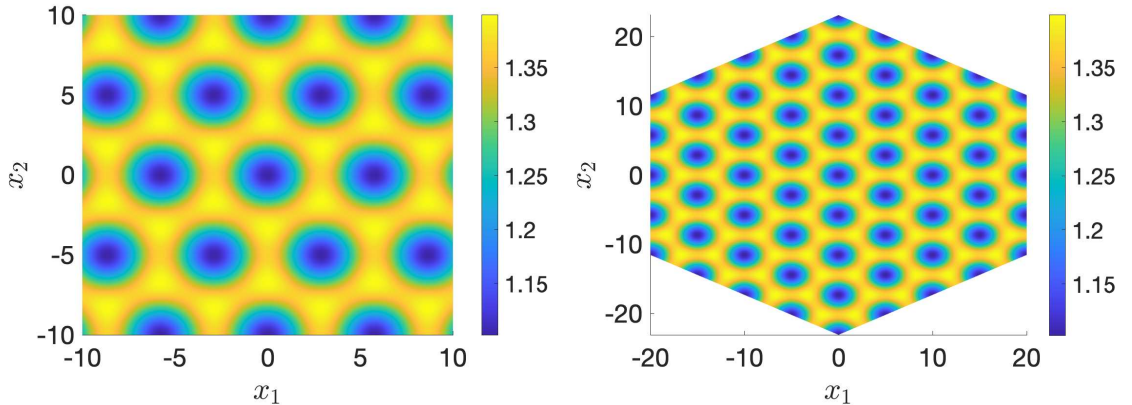


Figure 7: Plot of  $\bar{u}$  of an approximation of a  $D_6$  Pattern on  $(-10, 10)^2$  (L) and on  $\mathcal{O}_0$  (R).

**Theorem 3.11 (The Third Hexagonal Solution).** *Let  $\mu = 0.3, \gamma = 2.1$ . Moreover, let  $r_0 \stackrel{\text{def}}{=} 7 \times 10^{-5}$ . Then there exists a unique solution  $\tilde{u}$  to (5) in  $\overline{B_{r_0}(\bar{u})} \subset \ell_{6,1.4}^1$  and we have that  $\|\tilde{u} - u_0\|_{\mathcal{B}(\ell_{6,1.4}^1)} \leq r_0$ . Moreover,  $\tilde{u}$  is periodic on  $\mathcal{O}_0$ .*



*Proof.* Choose  $N = 16, d = 5$ . Then, we perform the full construction described in Section 3.2 to build  $\bar{u}$  and  $A^N$ . Using [4, 5], we choose  $r_0 \stackrel{\text{def}}{=} 7 \times 10^{-5}$  and obtain

$$\|A^N\|_{\mathcal{B}(\ell_{6,1.4}^1)} \leq 588.773, Y_0 \stackrel{\text{def}}{=} 3.83 \times 10^{-5}, Z_2(r_0) \stackrel{\text{def}}{=} 3404.11, Z_1 \stackrel{\text{def}}{=} 0.2686, Z_0 \stackrel{\text{def}}{=} 6.9233 \times 10^{-12}.$$

We prove that these values satisfy Theorem 3.1. □

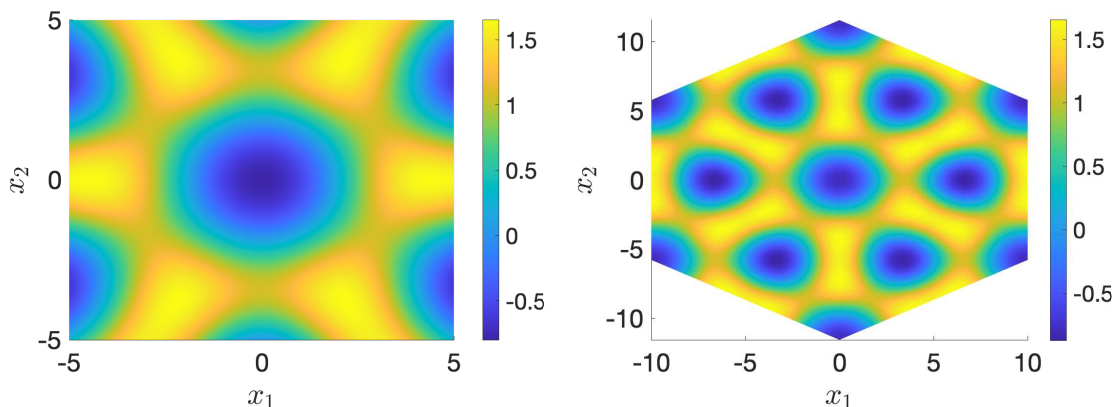


Figure 8: Plot of  $\bar{u}$  of an approximation of a  $D_6$  Pattern on  $(-5, 5)^2$  (L) and on  $\mathcal{O}_0$  (R).

**Theorem 3.12 (The Fourth Hexagonal Solution).** *Let  $\mu = 0.25, \gamma = 2$ . Moreover, let  $r_0 \stackrel{\text{def}}{=} 4 \times 10^{-5}$ . Then there exists a unique solution  $\tilde{u}$  to (5) in  $B_{r_0}(\bar{u}) \subset \ell_{6,1.09}^1$  and we have that  $\|\tilde{u} - u_0\|_{\ell_{6,1.09}^1} \leq r_0$ . Moreover,  $\tilde{u}$  is periodic on  $\mathcal{O}_0$ .*

*Proof.* Choose  $N = 56, d = 15$ . Then, we perform the full construction described in Section 3.2 to build  $\bar{u}$  and  $A^N$ . Using [4, 5], we choose  $r_0 \stackrel{\text{def}}{=} 4 \times 10^{-5}$  and obtain

$$\|A^N\|_{\mathcal{B}(\ell_{6,1.09}^1)} \leq 44.624, Y_0 \stackrel{\text{def}}{=} 4.543 \times 10^{-6}, Z_2(r_0) \stackrel{\text{def}}{=} 3773.54, Z_1 \stackrel{\text{def}}{=} 0.8061, Z_0 \stackrel{\text{def}}{=} 1.51 \times 10^{-10}.$$

We prove that these values satisfy Theorem 3.1. □

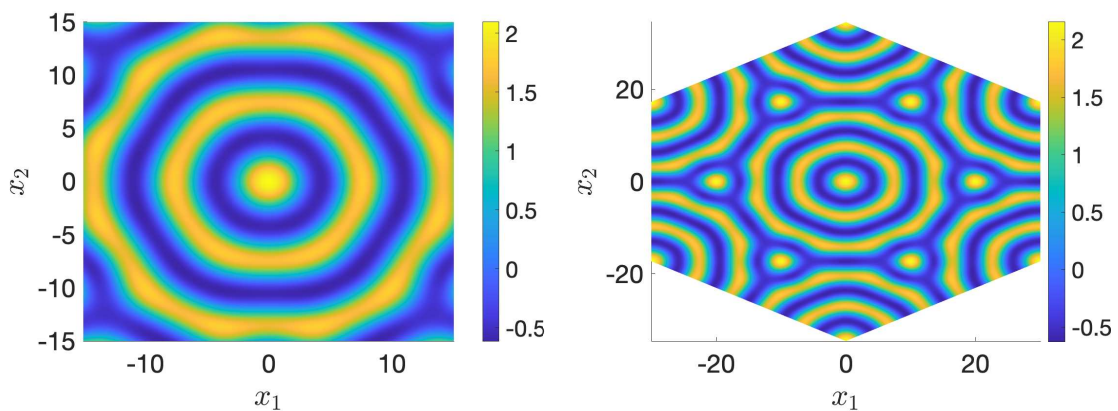


Figure 9: Plot of  $\bar{u}$  of an approximation of a  $D_6$  Pattern on  $(-15, 15)^2$  (L) and on  $\mathcal{O}_0$  (R).



## 4 Branches of Hexagonal and Triangular Solutions

In this section, we wish to prove the existence of a branch of periodic solutions whose periodic patterns can be generated by two triangles or one hexagon depending on the symmetry. There is a strong interest in branches of solutions in 2D Swift Hohenberg. In particular, the authors of [21] and [22] provide various approximate branches of solutions. Some of these branches emerge from a Turing bifurcation that lead to homoclinic snaking. Others form isolas of localized solutions. As shown in [26], various hexagonal patterns that fill the domain along the snaking curve are presented. Additionally, a rich variety of purely periodic patterns exist in (1) which both hexagonal and triangular symmetry. We would like to provide rigorous proofs of the symmetry of these branches of solutions. That is, we would like to prove that the branch itself is  $D_j$ -symmetric. This means that each solution along the branch is a periodic pattern that can be generated by two triangles (in the case of  $D_3$ ) or one hexagon (in the case of  $D_6$ ). Our approach will be computer-assisted and was developed by the authors of [11]. The approach is based on Chebyshev series, and allows us to parameterize the branch as a Chebyshev series expansion. It has been applied before in previous works, and we refer the interested reader to [12, 16] for examples.

For our purposes, we will be performing continuation in  $\mu$ . We will use pseudo-arclength continuation to perform our rigorous proof. The benefit of pseudo-arclength continuation is that we can pass through saddle node (or fold) bifurcations. We will require this in order to prove Theorems 4.8 and 4.9. To begin, we define  $X_{j,\nu} \stackrel{\text{def}}{=} \mathbb{R} \times \ell_{j,\nu}^1$  and write  $w \stackrel{\text{def}}{=} (\mu, u) \in X_{j,\nu}$ . Now, we will expand  $\mu$  and  $u$  as Chebyshev series dependent on the pseudo-arclength,  $s$ . That is, we write

$$\mu(s) \stackrel{\text{def}}{=} \mu_0 + 2 \sum_{n=1}^{N_c} \mu_n T_n(s) \quad \text{and} \quad u(s) \stackrel{\text{def}}{=} u_0 + 2 \sum_{n=1}^{N_c} u_n T_n(s), \quad s \in [-1, 1]$$

where  $T_n : [-1, 1] \rightarrow \mathbb{R}$  are the Chebyshev polynomials of the first kind and  $\mu_n \in \mathbb{R}, u_n \in \ell_{j,\nu}^1$  for all  $n \in \{0, \dots, N_{\text{cheb}}\}$ . We then write  $w(s) \stackrel{\text{def}}{=} (\mu(s), u(s)) \in \mathbb{R}_{\text{con}} \times \ell_{j,\nu,\text{con}}^1 \stackrel{\text{def}}{=} X_{j,\nu,\text{con}}$  where  $\mathbb{R}_{\text{con}}, \ell_{j,\nu,\text{con}}^1$  and  $X_{j,\nu,\text{con}}$  are Banach spaces with the norms

$$\begin{aligned} \|\mu(s)\|_{\mathbb{R}_{\text{con}}} &\stackrel{\text{def}}{=} |\mu_0| + 2 \sum_{n=1}^{N_c} |\mu_n|, \quad \|u(s)\|_{\ell_{j,\nu,\text{con}}^1} \stackrel{\text{def}}{=} \|u_0\|_{1,\nu} + 2 \sum_{j=1}^{N_c} \|u_n\|_{1,\nu}, \\ \|w(s)\|_{X_{j,\nu,\text{con}}} &\stackrel{\text{def}}{=} \|w_0\|_{X_{j,\nu}} + 2 \sum_{n=1}^{N_c} \|w_n\|_{X_{j,\nu}}. \end{aligned}$$

We then define the map  $F : X_{j,\nu,\text{con}} \rightarrow \mathcal{S}$  for  $\mathcal{S}$  another Banach space as

$$F(w(s)) \stackrel{\text{def}}{=} \begin{bmatrix} (u(s) - \bar{u}(s), \dot{u}(s))_2 \\ f(\mu(s), u(s)) \end{bmatrix} \quad (14)$$

where  $\dot{u}(s)$  is the second component of the *tangent vector*,  $\dot{w}(s)$ . We do the same for the approximate inverse, which we will denote by  $B(s) : \mathcal{S} \rightarrow X_{j,\nu,\text{con}}$

$$B(s) = B_0 + 2 \sum_{n=1}^{N_c} B_n T_n(s).$$

Note that in this case  $B(s)$  is an approximate inverse to  $DF(w(s))$ . Then, the following theorem makes use of a uniform contraction argument to allow us to rigorously prove a branch of solutions.

**Theorem 4.1** (Newton-Kantorovich Theorem for Branches). *Let  $B^\dagger(s) \in \mathcal{B}(X_{j,\nu,\text{con}}, \mathcal{S})$ . Also let  $B(s) \in \mathcal{B}(\mathcal{S}, X_{j,\nu,\text{con}})$  be injective. Moreover, let  $Y_0^{[s]}, Z_0^{[s]}, Z_1^{[s]}$  be non-negative constants and let*

$Z_2^{[s]} : (0, \infty) \rightarrow [0, \infty)$  be a non-negative function such that

$$\begin{aligned} \sup_{s \in [-1, 1]} \|B(s)F(\bar{w}(s))\|_{X_{j,\nu,con}} &\leq Y_0^{[s]} \\ \sup_{s \in [-1, 1]} \|I_d - B(s)B^\dagger(s)\|_{\mathcal{B}(X_{j,\nu,con})} &\leq Z_0^{[s]} \\ \sup_{s \in [-1, 1]} \|B(s)(DF(\bar{w}(s)) - B^\dagger(s))\|_{\mathcal{B}(X_{j,\nu,con})} &\leq Z_1^{[s]} \\ \sup_{s \in [-1, 1]} \|B(s)(DF(w(s)) - DF(\bar{w}(s)))\|_{\mathcal{B}(X_{j,\nu,con})} &\leq Z_2^{[s]}(r)r, \text{ for all } w(s) \in B_r(w_0(s)) \end{aligned}$$

If there exists  $r > 0$  such that

$$\frac{1}{2}Z_2^{[s]}(r)r^2 - (1 - Z_0^{[s]} - Z_1^{[s]})r + Y_0^{[s]} < 0, \text{ and } Z_0^{[s]} + Z_1^{[s]} + Z_2^{[s]}(r)r < 1$$

is satisfied, then for every  $s \in [-1, 1]$ , there exists a unique  $\tilde{w}(s) \in \overline{B_r(\bar{w}(s))} \subset X_{j,\nu,con}$  such that  $F(\tilde{w}(s)) = 0$ . Moreover, the function  $s \rightarrow \tilde{w}(s)$  is of class  $C^\infty$ .

*Proof.* The proof can be found in [10], [17], and [32] for instance. Similar to Remark 3.1, we do not specify the Banach space  $\mathcal{S}$  as it will not play a role in our estimates.  $\square$

Let us now discuss the numerical aspects of this approach in order to apply Theorem 4.1.

#### 4.1 Construction of $\bar{w}(s)$ , $B^\dagger(s)$ and $B(s)$

In this section, we will discuss the computation of  $\bar{w}(s)$ ,  $B^\dagger(s)$ , and  $B(s)$ . Our approach will rely on the Fast Fourier Transform (FFT) and numerical pseudo-arclength continuation. To compute each  $\bar{w}_n \stackrel{\text{def}}{=} (\bar{\mu}_n, \bar{u}_n)$ , we first choose the number of Chebyshev coefficients, denoted  $N_c$ . We will compute the next power of 2 after  $N_c$  and denote it by  $N_{FFT}$ . Following this, we fix an arclength, denoted  $s_{fix} \in \mathbb{R}^+$ , and create a grid of points

$$s_{grid,k} \stackrel{\text{def}}{=} \frac{1}{2}s_{fix} - \frac{1}{2}s_{fix} \cos\left(\frac{2\pi k}{N_{FFT}}\right) \text{ for } k = 0, \dots, \frac{N_{FFT}}{2} - 1.$$

The grid of  $s_{grid,k}$ 's is meant to give us the step-sizes for our pseudo-arclength continuation. That is, the step-size of each pseudo-arclength continuation step will be  $ds_k \stackrel{\text{def}}{=} s_{grid,k} - s_{grid,k-1}$ . To explain further, suppose we have obtained an approximate solution,  $\bar{w}_{grid,k} \stackrel{\text{def}}{=} (\bar{\mu}_{grid,k}, \bar{u}_{grid,k})$  to  $f(\bar{w}_{grid,k}) \approx 0$  and computed the tangent vector to the branch, denoted  $\dot{w}_{grid,k}$ . Then, we define

$$\bar{w}_{grid,k+1} \stackrel{\text{def}}{=} \bar{w}_{grid,k} \pm ds_k \dot{w}_{grid,k}$$

where we choose the sign of  $ds_k$  depending on the direction we wish to continue. We do this for all  $k = 0, \dots, \frac{N_{FFT}}{2} - 1$ . At this point, we have a grid of approximate solutions  $\bar{w}_{grid,k}$  for all  $k = 0, \dots, \frac{N_{FFT}}{2}$  to  $f(\bar{w}_{grid,k}) \approx 0$ . We then use an inverse Fast Fourier transform (IFFT) to compute the approximate branch of solutions  $\bar{w}(s) \stackrel{\text{def}}{=} (\bar{w}_n)_{n \in \{0, \dots, N_c\}}$ . To demonstrate the connection, we would approximately have

$$\bar{w}\left(\frac{2(s_{grid,k} - s_{fix})}{s_{fix}} + 1\right) \approx \bar{w}_{grid,k}, \text{ for } k = 0, \dots, \frac{N_{FFT}}{2} - 1$$

when evaluating at the grid points  $s_{grid,k}$ .

Let us now move to the discussion of  $B^\dagger(s)$  and  $B(s)$ . To begin, we would like to construct a grid of  $B_{grid,k}^\dagger$  and approximate inverses  $B_{grid,k}$  for  $k = 0, \dots, \frac{N_{FFT}}{2} - 1$ . That is, we would like to have  $B_{grid,k}^\dagger \approx DF(\bar{w}_{grid,k})$  and  $B_{grid,k} \approx DF(\bar{w}_{grid,k})^{-1}$  for each  $k$ . We first define some notations. We introduce  $\Pi^N, \Pi_N$  and  $\mathfrak{h}_n$  for  $\mathfrak{h} \stackrel{\text{def}}{=} (\eta, h) \in X_{j,\nu}$ . These are

$$\Pi^N \stackrel{\text{def}}{=} \begin{bmatrix} 1 & 0 \\ 0 & \pi^N \end{bmatrix}, \quad \Pi_N \stackrel{\text{def}}{=} \begin{bmatrix} 0 & 0 \\ 0 & \pi_N \end{bmatrix}, \quad (\mathfrak{h})_n \stackrel{\text{def}}{=} (\eta, h_n).$$

Then, we define the action of  $B_{grid,k}^\dagger$  as

$$(B_{grid,k}^\dagger \mathbf{h})_n \stackrel{\text{def}}{=} \begin{cases} [\Pi^N DF(\bar{w}_{grid,k}) \Pi^N \mathbf{h}]_n & n \in I^N \\ \begin{bmatrix} 0 \\ ((1 + |\mathcal{L}\tilde{n}|^2)^2 + \bar{\mu}_{grid,k})h_n \end{bmatrix} & n \in \mathbb{Z}^2 \setminus I^N \end{cases}$$

Following this, we choose  $B_{grid,k}^N \approx (\Pi^N DF(\bar{w}_{grid,k}) \Pi^N)^{-1}$  and then each  $B_{grid,k}$  is defined as

$$(B_{grid,k} \mathbf{h})_n \stackrel{\text{def}}{=} \begin{cases} (B_{grid,k}^N \Pi^N \mathbf{h})_n & n \in I^N \\ \begin{bmatrix} 0 \\ \frac{h_n}{(1 + |\mathcal{L}\tilde{n}|^2)^2 + \bar{\mu}_{grid,k}} \end{bmatrix} & n \in \mathbb{Z}^2 \setminus I^N \end{cases}.$$

Note that the tail is chosen exactly as was previously done for  $A$  in Section 3.2. That difference is that we are on a product space,  $X_{j,\nu}$ . As a result, we needed to introduce the extra component. At this point, we now use the IFFT again to compute the approximate branch of  $B^\dagger(s)$  and approximate inverses  $B(s)$ . As before, we would approximately have

$$B^\dagger \left( \frac{2(s_{grid,k} - s_{fix})}{s_{fix}} + 1 \right) \approx B_{grid,k}^\dagger, \quad B \left( \frac{2(s_{grid,k} - s_{fix})}{s_{fix}} + 1 \right) \approx B_{grid,k}, \quad \text{for } k = 0, \dots, \frac{N_{FFT}}{2} - 1$$

when evaluating at the grid points  $s_{grid,k}$ . Finally, we need an estimate for  $\|\Pi_N B(s)\|_{\mathcal{B}(X_{j,\nu,con})}$ . To begin, notice that

$$\|\Pi_N B(s)\|_{\mathcal{B}(X_{j,\nu,con})} = \|\Pi_N B_0\|_{X_{j,\nu}} + 2 \sum_{n=1}^{N_c} \|\Pi_N B_n\|_{X_{j,\nu}}.$$

Now, for each  $k$ , we would have

$$\|\Pi_N B_n\|_{X_{j,\nu}} \leq \max_{m \in \mathbb{Z}^2 \setminus I^N} \frac{1}{|(1 + |\mathcal{L}\tilde{m}|^2)^2 + \bar{\mu}_n|} \leq \max_{k \in \{0,1,\dots,N_c\}} \max_{m \in \mathbb{Z}^2 \setminus I^N} \frac{1}{|(1 + |\mathcal{L}\tilde{m}|^2)^2 + \bar{\mu}_k|} \stackrel{\text{def}}{=} \frac{1}{L_{N,K}},$$

where

$$L_{N,K} \stackrel{\text{def}}{=} \min_{k \in \{0,1,\dots,N_c\}} \min_{m \in \mathbb{Z}^2 \setminus I^N} |(1 + |\mathcal{L}\tilde{m}|^2)^2 + \bar{\mu}_k|. \quad (15)$$

The final estimate is so that we can obtain a uniform bound. Indeed, we obtain

$$\|\Pi_N B(s)\|_{\mathcal{B}(X_{j,\nu,con})} = \|\Pi_N B_0\|_{X_{j,\nu}} + 2 \sum_{n=1}^{N_c} \|\Pi_N B_n\|_{X_{j,\nu}} \leq \frac{1}{L_{N,K}} + 2 \sum_{n=1}^{N_c} \frac{1}{L_{N,K}} = \frac{2N_c + 1}{L_{N,K}}.$$

This is a description of the numerical tools needed in order to apply Theorem 4.1. Let us now discuss the computation of the bounds.

## 4.2 Computing the Bounds for Branches of Solutions

In this section, we will compute the bounds  $Y_0^{[s]}$ ,  $Z_0^{[s]}$ ,  $Z_1^{[s]}$ , and  $Z_2^{[s]}(r)$ . These computations will be similar to those done in Section 3.3, but involve the use of the FFT. First, let us introduce some notation. Let  $\mathcal{F}_{\mathcal{N}}[\cdot]$  denote the Fourier transform with  $\mathcal{N}$  coefficients of a Chebyshev sequence. That is, for a chosen  $\mathcal{N}$  we will compute the next power of 2 and zero pad the Chebyshev sequence if necessary. Then we take the Chebyshev FFT. We similarly define  $\mathcal{F}_{\mathcal{N}}^{-1}[\cdot]$  to be the analogous definition for the IFFT. At this point, we also define pointwise multiplication, denoted  $.*$  as

$$w(s) .* z(s) \stackrel{\text{def}}{=} (w_0 z_0, w_1 z_1, \dots, w_{\mathcal{N}} z_{\mathcal{N}}) \quad \text{where } (w(s))_{n \in \{0,\dots,\mathcal{N}\}}, (z(s))_{n \in \{0,\dots,\mathcal{N}\}}.$$

We are now ready compute  $Y_0^{[s]}$  and  $Z_0^{[s]}$ .

**Lemma 4.2.** Let  $L_{N,K}$  be defined as in (15). Let  $Y_0^{[s]}, Z_0^{[s]}$  be defined as

$$Y_0^{[s]} \stackrel{\text{def}}{=} \|\mathcal{F}_{4N_c}^{-1}[\mathcal{F}_{4N_c}[B^N(s)] \cdot * F(\mathcal{F}_{4N_c}[\bar{w}(s)])]\|_{X_{j,\nu,\text{con}}} + \frac{2N_c+1}{L_{N,K}} \left\| \mathcal{F}_{3N_c}^{-1}[(\pi^{3N} - \pi^N)G(\mathcal{F}_{3N_c}[\bar{w}(s)])] \right\|_{\ell_{j,\nu,\text{con}}^1}.$$

$$Z_0^{[s]} \stackrel{\text{def}}{=} \|\mathcal{F}_{2N_c}^{-1}[\Pi^N - \mathcal{F}_{2N_c}[B^N(s)] \cdot * \mathcal{F}_{2N_c}[\Pi^N DF(\bar{w}(s))\Pi^N]]\|_{\mathcal{B}(X_{j,\nu,\text{con}})}.$$

Then, we have  $\sup_{s \in [-1,1]} \|B(s)F(\bar{w}(s))\|_{X_{j,\nu,\text{con}}} \leq Y_0^{[s]}$  and  $\|I_d - B(s)B^\dagger(s)\|_{\mathcal{B}(X_{j,\nu,\text{con}})} = Z_0^{[s]}$ .

*Proof.* Beginning with  $Y_0^{[s]}$ , observe that we can write

$$\begin{aligned} \|B(s)F(\bar{w}(s))\|_{X_{j,\nu,\text{con}}} &\leq \|\Pi^N B(s)F(\bar{w}(s))\|_{X_{j,\nu,\text{con}}} + \|\Pi_N B(s)F(\bar{w}(s))\|_{X_{j,\nu,\text{con}}} \\ &\leq \|B^N(s)F(\bar{w}(s))\|_{X_{j,\nu,\text{con}}} + \|\Pi_N B(s)\|_{\mathcal{B}(X_{j,\nu,\text{con}})} \left\| \begin{bmatrix} 0 \\ \pi_N f(\bar{w}(s)) \end{bmatrix} \right\|_{X_{j,\nu,\text{con}}} \\ &= \|B^N(s)F(\bar{w}(s))\|_{X_{j,\nu,\text{con}}} + \frac{2N_c+1}{L_{N,K}} \|(\pi^{3N} - \pi^N)G(\bar{w}(s))\|_{\ell_{j,\nu,\text{con}}^1} \end{aligned}$$

We must now compute the pointwise products, which we will do this using the FFT. With respect to  $s$ ,  $B^N(s)$  is a polynomial of order  $N_c$  and  $F(\bar{w}(s))$  is a polynomial of order  $3N_c$ . Hence, it follows that  $B(s)F(\bar{w}(s))$  is a polynomial of order  $4N_c$  with respect to  $s$ . Therefore, we will use  $4N_c$  Chebyshev coefficients when computing our Fourier transforms for this term. Moreover,  $G(\bar{w}(s))$  is a polynomial of order  $3N_c$ , so we can use  $3N_c$  for this Fourier transform. Once we have found this, we can directly apply the result of Lemma 3.2 for  $Y_0$  to obtain the estimate.

For  $Z_0^{[s]}$ , similarly as in Lemma 3.2, the tails of  $B(s)$  and  $B^\dagger(s)$  cancel exactly. This leave us with with the finite parts. Note that  $B^N(s)$  and  $\Pi^N DF(\bar{w}(s))\Pi^N$  are polynomials of order  $N_c$ . Hence, it follows that  $B^N(s)\Pi^N DF(\bar{w}(s))\Pi^N$  is a polynomial of order  $2N_c$  with respect to  $s$ . Therefore, we use  $2N_c$  Chebyshev coefficients when computing our Fourier transforms. Once we have this, we directly apply the result of Lemma 3.2 to obtain the estimate.  $\square$

Next, we must compute  $Z_2^{[s]}(r)$ . Let us state the lemma for it.

**Lemma 4.3.** Let  $q(s) = (q_n)_{n \in \{0, \dots, N_c\}}$  and each  $q_n$  is a Fourier series with  $k$ th coefficient  $(q_n)_k = -2\gamma\delta_k + 6(\bar{u}_n)_k$  where  $\bar{u}(s) = (\bar{u}_n)_{n \in \{0, \dots, N_c\}}$ ,  $(\bar{u}_n)_k$  is the  $k$ th Fourier coefficient, and  $\delta_k$  is the Kronecker delta. Let  $L_{N,K}$  be defined as in (15). Now, let  $Z_2^{[s]}(r) : (0, \infty) \rightarrow [0, \infty)$  be defined as

$$Z_2^{[s]}(r) \stackrel{\text{def}}{=} \left( \|B^N(s)\|_{\mathcal{B}(X_{j,\nu,\text{con}})} + \frac{2N_c+1}{L_{N,K}} \right) \left( 1 + \|q(s)\|_{\ell_{j,\nu,\text{con}}^1} + 3r \right).$$

Then, it follows that  $\sup_{s \in [-1,1]} \|B(s)(DF(w(s)) - DF(\bar{w}(s)))\|_{\mathcal{B}(X_{j,\nu,\text{con}})} \leq Z_2^{[s]}(r)r$ .

*Proof.* To begin, since  $w(s) \in B_r(\bar{w}(s))$ , there exists a  $v(s) \in B_r(0)$  such that  $w(s) = \bar{w}(s) + v(s)$ . Note that  $\|v(s)\|_{\ell_{j,\nu,\text{con}}^1} \leq r$ . The proof now follows similar steps to those used in Lemma 3.3. That is, we obtain

$$\begin{aligned} \|B(s)(DF(w(s)) - DF(\bar{w}(s)))\|_{\mathcal{B}(X_{j,\nu,\text{con}})} &\leq \|B(s)\|_{\mathcal{B}(X_{j,\nu,\text{con}})} \left\| \begin{bmatrix} 0 & 0 \\ -v(s) & q(s)v(s) + 3v(s)^2 \end{bmatrix} \right\|_{\mathcal{B}(X_{j,\nu,\text{con}})} \\ &\leq \left( \|B^N(s)\|_{\mathcal{B}(X_{j,\nu,\text{con}})} + \frac{2N_c+1}{L_{N,K}} \right) \left( \|v(s)\|_{\mathcal{B}(\mathbb{R}_{\text{con}}, \ell_{k,\nu,\text{con}}^1)} + \|q(s)v(s)\|_{\mathcal{B}(\ell_{j,\nu,\text{con}}^1)} + 3\|v(s)\|_{\mathcal{B}(\ell_{j,\nu,\text{con}}^1)}^2 \right) \\ &\leq \left( \|B^N(s)\|_{\mathcal{B}(X_{j,\nu,\text{con}})} + \frac{2N_c+1}{L_{N,K}} \right) \left( r + \|q(s)\|_{\ell_{j,\nu,\text{con}}^1} r + 3r^2 \right) \stackrel{\text{def}}{=} Z_2^{[s]}(r)r \end{aligned}$$

where we used that  $\ell_{j,\nu,\text{con}}^1$  is a Banach algebra and similar steps to those used in Lemma 3.3 to obtain the estimate on  $\|B(s)\|_{\mathcal{B}(X_{j,\nu,\text{con}})}$ . This concludes the proof.  $\square$

Finally, we compute the  $Z_1^{[s]}$  bound. First, we will define  $\bar{v}(s) \in \ell_{j,\nu,\text{con}}^1$  as

$$\bar{v}(s) \stackrel{\text{def}}{=} -2\gamma\bar{u}(s) + 3\mathcal{F}_{2N_c}^{-1}[\mathcal{F}_{2N_c}[\bar{u}(s)] \cdot * \mathcal{F}_{2N_c}[\bar{u}(s)]].$$

Note that  $\bar{u}(s)$  is a polynomial of order  $N_c$  with respect to  $s$ . Hence, we expect  $\bar{u}(s)^2$  to be a polynomial of order  $2N_c$  with respect to  $s$ , so we choose our FFT size appropriately. We now state the result for  $Z_1^{[s]}$  as a lemma.

**Lemma 4.4.** *Let  $L_{N,K}$  be defined as in (15). Let  $Z_1^{[s]} > 0$  be defined as*

$$Z_1^{[s]} \stackrel{\text{def}}{=} \left\| B^N(s) \begin{bmatrix} 0 \\ \phi(s) \end{bmatrix} \right\|_{X_{j,\nu,\text{con}}} + \frac{2N_c + 1}{L_{N,K}} \|\bar{v}(s)\|_{\ell_{j,\nu,\text{con}}^1}.$$

Then, it follows that  $\sup_{s \in [-1,1]} \|B(s)(DF(\bar{w}(s)) - B^\dagger(s))\|_{\mathcal{B}(X_{j,\nu,\text{con}})} \leq Z_1^{[s]}$ .

*Proof.* To begin, let  $\mathfrak{h}(s) \stackrel{\text{def}}{=} (\eta(s), h(s)) \in X_{j,\nu,\text{con}}$ . Observe that

$$\begin{aligned} (DF(\bar{w}(s)) - B^\dagger(s))\mathfrak{h}(s) &= \begin{bmatrix} (h(s), \dot{u}(s))_2 \\ \eta(s)\bar{u}(s) + Df(\bar{w}(s))h(s) \end{bmatrix} - \begin{bmatrix} (h(s), \dot{u}(s)\pi^N)_2 \\ \eta(s)\pi^N\bar{u}(s) + \pi^N Df(\bar{w}(s))\pi^N h(s) \end{bmatrix} \\ &= \begin{bmatrix} (h(s), \dot{u}(s) - \dot{u}(s)\pi^N)_2 \\ \eta(s)(\bar{u}(s) - \pi^N\bar{u}(s)) + (Df(\bar{w}(s)) - \pi^N Df(\bar{w}(s))\pi^N)h(s) \end{bmatrix} \\ &= \begin{bmatrix} 0 \\ (Df(\bar{w}(s)) - \pi^N Df(\bar{w}(s))\pi^N)h(s) \end{bmatrix} \end{aligned}$$

where the last step followed from the fact that  $\pi^N\bar{u}(s) = \bar{u}(s)$ ,  $\dot{u}(s)\pi^N = \dot{u}(s)$  by definition. Hence, we introduce  $z(s) \stackrel{\text{def}}{=} (Df(\bar{w}(s)) - \pi^N Df(\bar{w}(s))\pi^N)h(s)$  and write

$$\begin{aligned} \|B(s)(DF(\bar{w}(s)) - B^\dagger(s))\|_{\mathcal{B}(X_{j,\nu,\text{con}})} &= \left\| B(s) \begin{bmatrix} 0 \\ z(s) \end{bmatrix} \right\|_{X_{j,\nu,\text{con}}} \\ &= \left\| B^N(s) \begin{bmatrix} 0 \\ z(s) \end{bmatrix} \right\|_{X_{j,\nu,\text{con}}} + \left\| \Pi_N B(s) \begin{bmatrix} 0 \\ z(s) \end{bmatrix} \right\|_{X_{j,\nu,\text{con}}} \\ &\leq \left\| B^N(s) \begin{bmatrix} 0 \\ \bar{v}(s)\pi_N h(s) \end{bmatrix} \right\|_{X_{j,\nu,\text{con}}} + \|\Pi_N B(s)\|_{\mathcal{B}(X_{j,\nu,\text{con}})} \left\| \Pi_N \begin{bmatrix} 0 \\ z(s) \end{bmatrix} \right\|_{X_{j,\nu,\text{con}}} \\ &\leq \left\| B^N(s) \begin{bmatrix} 0 \\ \phi(s) \end{bmatrix} \right\|_{X_{j,\nu,\text{con}}} + \frac{2N_c + 1}{L_{N,K}} \|\bar{v}(s)\|_{\ell_{j,\nu,\text{con}}^1} \stackrel{\text{def}}{=} Z_1^{[s]} \end{aligned}$$

as desired.  $\square$

This concludes the computation of the bounds needed to apply Theorem 4.1. We are now able to prove the existence of symmetric branches of solutions periodic on a triangle and hexagon.

### 4.3 Hexagonal and Triangular Branches of Periodic Solutions

In this section, we present the proofs of five branches of solutions in (1). The first two will possess  $D_3$ -symmetry, meaning each periodic pattern on the branch can be generated by tiling with  $\Delta_1$  and  $\Delta_2$  according to Theorem 2.2. The latter three will possess  $D_6$ -symmetry, meaning each solution on the branch is periodic on  $\mathcal{O}_0$  according to Theorem 2.3. We now present the results.

**Theorem 4.5 (The First Triangular Branch).** *Let  $s_{fix} = 0.05, \gamma = 1.6, j = 3, \nu = 1.1$ . Moreover, let  $r_0 \stackrel{\text{def}}{=} 2 \times 10^{-5}$ . Then there exists a unique solution  $\tilde{w}(s)$  to (14) in  $\overline{B_{r_0}(\bar{w}(s))} \subset X_{3,1.1,\text{con}}$  and we have that  $\sup_{s \in [-1,1]} \|\tilde{w}(s) - \bar{w}(s)\|_{X_{3,1.1,\text{con}}} \leq r_0$ . This corresponds to a branch of periodic solutions in (1) under which the pattern can be generated by a tiling of  $\Delta_1$  and  $\Delta_2$ .*

*Proof.* Choose  $N = 40, d = 5, N_c = 3$ . Then, we perform the full construction described in Section 4.1 to build  $\bar{w}(s)$  and  $B^N(s)$ . Using [4, 5], we choose  $r_0 \stackrel{\text{def}}{=} 2 \times 10^{-5}$  and obtain

$$\|B^N(s)\|_{\mathcal{B}(X_{3,1.1,\text{con}})} \leq 113.916, Y_0 \stackrel{\text{def}}{=} 7.163 \times 10^{-6}, Z_2(r_0) \stackrel{\text{def}}{=} 11174.51, Z_1 \stackrel{\text{def}}{=} 0.4775, Z_0 \stackrel{\text{def}}{=} 0.02671.$$

We prove that these values satisfy Theorem 4.1.  $\square$

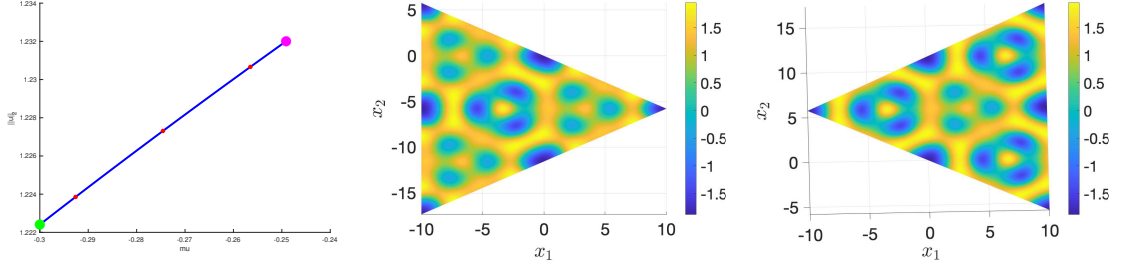


Figure 10: Plot of the branch of approximate solutions proven in Swift Hohenberg with  $D_3$ -symmetry (L). The approximation on the branch (magenta point) when  $\mu \approx -0.24913$  on  $\Delta_1$  (C) and  $\Delta_2$  (R).

**Theorem 4.6 (The Second Triangular Branch).** *Let  $s_{fix} = 0.5, \gamma = 0.3, j = 3, \nu = 1.4$ . Moreover, let  $r_0 \stackrel{\text{def}}{=} 2 \times 10^{-6}$ . Then there exists a unique solution  $\tilde{w}(s)$  to (14) in  $\overline{B_{r_0}(\bar{w}(s))} \subset X_{3,1.4,\text{con}}$  and we have that  $\sup_{s \in [-1,1]} \|\tilde{w}(s) - \bar{w}(s)\|_{X_{3,1.4,\text{con}}} \leq r_0$ . This corresponds to a branch of periodic solutions in (1) under which the pattern can be generated by a tiling of  $\Delta_1$  and  $\Delta_2$ .*

*Proof.* Choose  $N = 24, d = 5, N_c = 31$ . Then, we perform the full construction described in Section 4.1 to build  $\bar{w}(s)$  and  $B^N(s)$ . Using [4, 5], we choose  $r_0 \stackrel{\text{def}}{=} 2 \times 10^{-6}$  and obtain

$$\|B^N(s)\|_{\mathcal{B}(X_{3,1.4,\text{con}})} \leq 3241.65, Y_0 \stackrel{\text{def}}{=} 8.4 \times 10^{-7}, Z_2(r_0) \stackrel{\text{def}}{=} 257070.1, Z_1 \stackrel{\text{def}}{=} 0.1695, Z_0 \stackrel{\text{def}}{=} 8.063 \times 10^{-3}.$$

We prove that these values satisfy Theorem 4.1.  $\square$

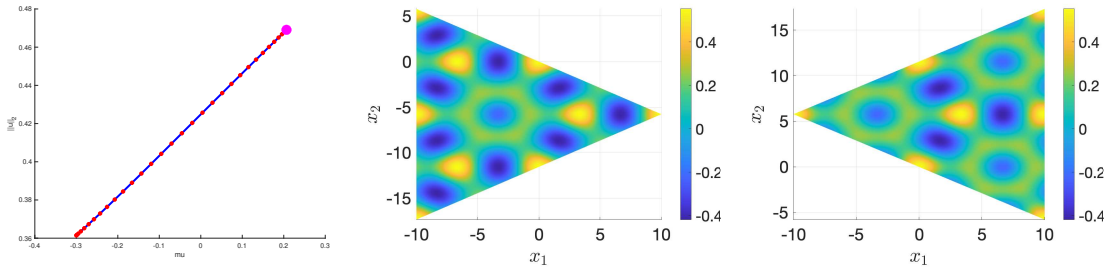


Figure 11: Plot of the branch of approximate solutions proven in Swift Hohenberg with  $D_3$ -symmetry (L). The approximation on the branch (magenta point) when  $\mu \approx 0.206565$  on  $\Delta_1$  (C) and  $\Delta_2$  (R).

We now present the proof of the hexagonal branch of solutions.

**Theorem 4.7 (The First Hexagonal Branch).** *Let  $s_{fix} = 0.4, \gamma = 1.6, j = 6, \nu = 1.1$ . Moreover, let  $r_0 \stackrel{\text{def}}{=} 1 \times 10^{-4}$ . Then there exists a unique solution  $\tilde{w}(s)$  to (14) in  $\overline{B_{r_0}(\bar{w}(s))} \subset X_{6,1.1,\text{con}}$  and we have that  $\sup_{s \in [-1,1]} \|\tilde{w}(s) - \bar{w}(s)\|_{X_{6,1.1,\text{con}}} \leq r_0$ . This corresponds to a branch of periodic solutions on  $\mathcal{O}_0$  to (1).*

*Proof.* Choose  $N = 60, d = 10, N_c = 7$ . Then, we perform the full construction described in Section 4.1 to build  $\bar{w}(s)$  and  $B^N(s)$ . Using [4, 5], we choose  $r_0 \stackrel{\text{def}}{=} 1 \times 10^{-4}$  and obtain

$$\|B^N(s)\|_{\mathcal{B}(X_{6,1.1,con})} \leq 45.28, Y_0 \stackrel{\text{def}}{=} 4.999 \times 10^{-5}, Z_2(r_0) \stackrel{\text{def}}{=} 3957.78, Z_1 \stackrel{\text{def}}{=} 0.239, Z_0 \stackrel{\text{def}}{=} 1.005 \times 10^{-2}.$$

We prove that these values satisfy Theorem 4.1.  $\square$

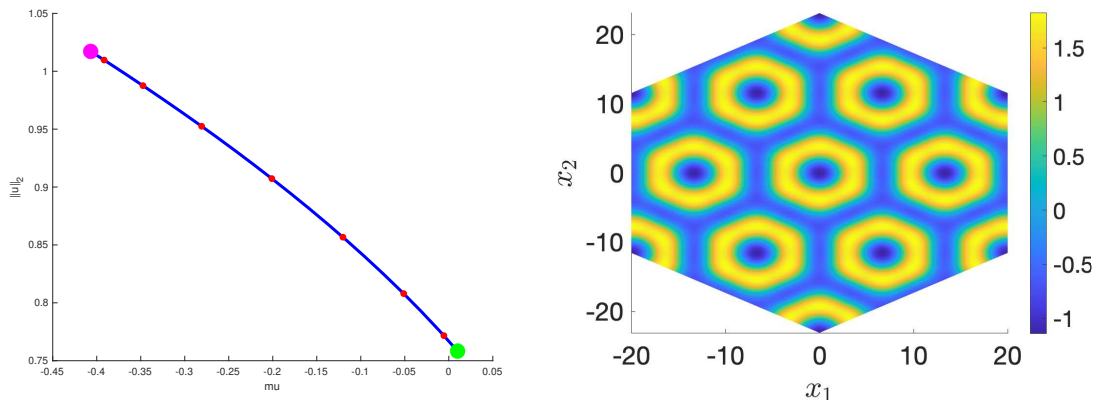


Figure 12: Plot of the branch of approximate solutions proven in Swift Hohenberg with  $D_6$ -symmetry (L). An approximate solution on the branch (magenta point) when  $\mu \approx -0.407$  (R).

**Theorem 4.8 (The Second Hexagonal Branch).** *Let  $s_{fix} = 0.18, \gamma = 1.6, j = 6, \nu = 1.25$ . Moreover, let  $r_0 \stackrel{\text{def}}{=} 5 \times 10^{-5}$ . Then there exists a unique solution  $\tilde{w}(s)$  to (14) in  $\overline{B_{r_0}(\bar{w}(s))} \subset X_{6,1.25,con}$  and we have that  $\sup_{s \in [-1,1]} \|\tilde{w}(s) - \bar{w}(s)\|_{X_{6,1.25,con}} \leq r_0$ . This corresponds to a branch of periodic solutions on  $\mathcal{O}_0$  to (1).*

*Proof.* Choose  $N = 20, d = 5, N_c = 31$ . Then, we perform the full construction described in Section 4.1 to build  $\bar{w}(s)$  and  $B^N(s)$ . Using [4, 5], we choose  $r_0 \stackrel{\text{def}}{=} 5 \times 10^{-5}$  and obtain

$$\|B^N(s)\|_{\mathcal{B}(X_{6,1.25,con})} \leq 36.122, Y_0 \stackrel{\text{def}}{=} 2.12 \times 10^{-5}, Z_2(r_0) \stackrel{\text{def}}{=} 8236.77, Z_1 \stackrel{\text{def}}{=} 0.2195, Z_0 \stackrel{\text{def}}{=} 0.03361.$$

We prove that these values satisfy Theorem 4.1.  $\square$

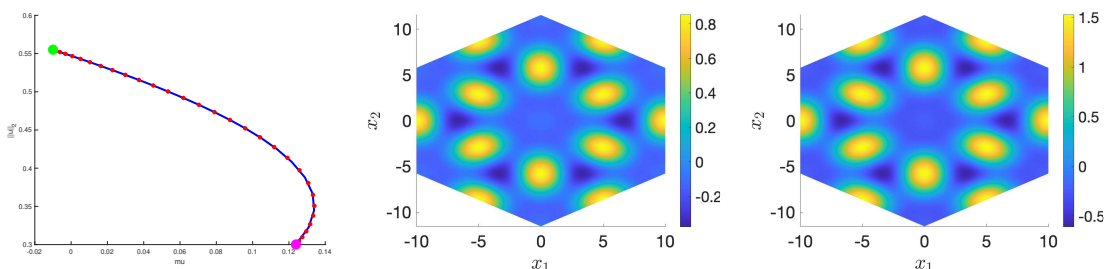


Figure 13: Plot of the branch of approximate solutions proven in Swift Hohenberg with  $D_6$ -symmetry (L). An approximate solution on the branch (magenta point) when  $\mu \approx 0.12385$  (C). An approximate solution on the branch (green point) when  $\mu \approx -0.01$  (R).

**Theorem 4.9 (The Third Hexagonal Branch).** *Let  $s_{fix} = 0.23, \gamma = 1.6, j = 6, \nu = 1.25$ . Moreover, let  $r_0 \stackrel{\text{def}}{=} 3 \times 10^{-5}$ . Then there exists a unique solution  $\tilde{w}(s)$  to (14) in  $\overline{B_{r_0}(\bar{w}(s))} \subset X_{6,1.25,con}$  and we have that  $\sup_{s \in [-1,1]} \|\tilde{w}(s) - \bar{w}(s)\|_{X_{6,1.25,con}} \leq r_0$ . This corresponds to a branch of periodic solutions on  $\mathcal{O}_0$  to (1).*

*Proof.* Choose  $N = 20$ ,  $d = 5$ ,  $N_c = 15$ . Then, we perform the full construction described in Section 4.1 to build  $\bar{w}(s)$  and  $B^N(s)$ . Using [4, 5], we choose  $r_0 \stackrel{\text{def}}{=} 3 \times 10^{-5}$  and obtain

$$\|B^N(s)\|_{\mathcal{B}(X_{6,1,25,con})} \leq 44.04, Y_0 \stackrel{\text{def}}{=} 8.204 \times 10^{-6}, Z_2(r_0) \stackrel{\text{def}}{=} 6065.53, Z_1 \stackrel{\text{def}}{=} 0.4403, Z_0 \stackrel{\text{def}}{=} 0.1857.$$

We prove that these values satisfy Theorem 4.1.  $\square$

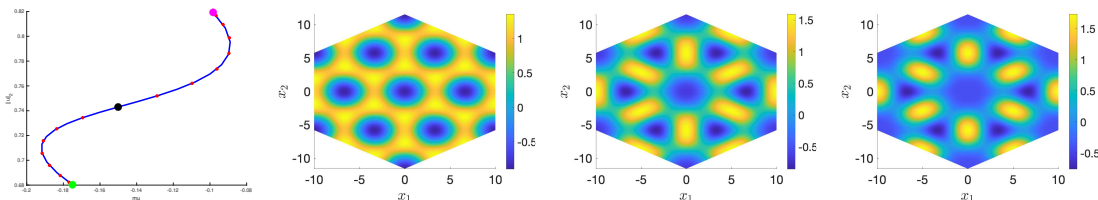


Figure 14: Plot of the branch of approximate solutions proven in Swift Hohenberg with  $D_6$ -symmetry (L). An approximate solution on the branch (magenta point) when  $\mu \approx -0.0983$  (ML). An approximate solution on the branch (black point) when  $\mu \approx -0.1501$  (MR). An approximate solution on the branch (green point) when  $\mu \approx -0.175$  (R).

## 5 Conclusion

In this paper, we provided an approach for rigorously proving the existence, local uniqueness, and  $D_j$  for  $j = 3, 6$  symmetry of periodic solutions to the 2D Swift Hohenberg PDE. We provided the necessary tools via [5] for performing the computer assisted proof using [23]. Additionally, for  $D_3$ , we showed that we can generate the periodic tiling via two triangles invariant under  $D_3$ -symmetry. For  $D_6$ , we showed that the same result can be obtained with only one hexagon leading to a periodic function defined on a hexagon.

There are many future works that could build on our approach. The first is related to the approach developed by the authors of [6]. In their methodology, it is a requirement that the Fourier series of  $u_0$  is on the square lattice. The problematic is that this method requires one to consider the domain  $\square_0$  and extend the function by 0 on  $\mathbb{R}^2$  rather than periodically. Since the domain  $\square_0$  itself is not invariant under  $D_3$  nor  $D_6$ -symmetry, one cannot construct an approximate solution of a localized pattern this way. This means the authors cannot utilize the useful symmetry reduction that hexagonal lattice symmetries provide, which would be particularly helpful when proving localized patterns as they are often more computationally intensive. Furthermore, it was shown by the authors of [15] that along with the localized pattern, we obtain a proof of a branch of periodic solutions converging to the localized pattern. Currently, this branch of periodic solutions would be on the square due to the fact that the method developed in [6] requires a Fourier series posed on the square lattice. Since hexagons tile the plane, and we only need one hexagon to generate the periodic tiling, taking the limit as the period tends to infinity, one can expect related localized patterns. This would make it of great interest to combine the approaches, and we consider it future work to obtain a branch of periodic solutions on a hexagon converging to a  $D_6$  localized pattern.

Another possible interest is computational. In its current form, the sequence structures for  $D_3$  and  $D_6$  have many indices which are of zero value. Since many operations, particularly convolution, are done by looping over all of  $I^N$ , there are many extra loop iterations being performed that are unnecessary. The ability to improve this would make the use of [5] of higher interest for more computationally intensive problems.

## References

- [1] M. Beck, J. Knobloch, D. J. B. Lloyd, B. Sandstede, and T. Wagenknecht. Snakes, ladders, and isolas of localized patterns. *SIAM J. Math. Anal.*, 41(3):936–972, 2009.



- [2] L. Benet and D. Sanders. Intervalarithmic.jl, 2022. <https://github.com/JuliaIntervals/IntervalArithmetic.jl>.
- [3] D. Blanco. D4Fourier.jl, 2024. <https://github.com/dominicblanco/D4Fourier.jl>.
- [4] D. Blanco. D3D6solutionSH.jl, 2026. <https://github.com/dominicblanco/D3D6solutionsSH.jl>.
- [5] D. Blanco. dihedral.jl, 2026. <https://github.com/dominicblanco/dihedral.jl>.
- [6] D. Blanco and M. Cadiot. Proving symmetry of localized solutions and application to dihedral patterns in the planar Swift-Hohenberg PDE. <https://arxiv.org/abs/2509.10375>, 2025.
- [7] G. M. Boissoniere, R. Choksi, and J.-P. Lessard. Microscopic patterns in the 2D phase-field crystal model. *Nonlinearity*, 35:1500–1520, 2022.
- [8] J. Bramburger, D. Hill, and D. Lloyd. Localized Patterns. <https://arxiv.org/abs/2404.14987> (Accepted to *SIAM*), 2024.
- [9] J. J. Bramburger, D. Altschuler, C. I. Avery, T. Sangsawang, M. Beck, P. Carter, and B. Sandstede. Localized radial roll patterns in higher space dimensions. *SIAM J. Appl. Dyn. Syst.*, 18(3):1420–1453, 2019.
- [10] M. Bredan, J.-P. Lessard, and M. Vanicat. Global bifurcation diagrams of steady states of systems of PDEs via rigorous numerics: a 3-component reaction-diffusion system. *Acta Applicandae Mathematicae*, 128(1):113–152, 2013.
- [11] M. Breden. A Posteriori Validation of Generalized Polynomial Chaos Expansions. *SIAM Journal on Applied Dynamical Systems*, 22(2):765–801, 2023.
- [12] M. Cadiot. Constructive proofs of existence and stability of solitary waves in the Whitham and capillary-gravity Whitham equations. *Nonlinearity*, 38(3):035021, 2025.
- [13] M. Cadiot and D. Blanco. Localized stationary patterns in the 2D Gray Scott model: computer-assisted proofs of existence. *Nonlinearity*, 38(4):045016, 2025.
- [14] M. Cadiot, J.-P. Lessard, and J.-C. Nave. Rigorous Computation of Solutions of Semilinear PDEs on Unbounded Domains via Spectral Methods. *SIAM Journal on Applied Dynamical Systems*, 23(3):1966–2017, 2024.
- [15] M. Cadiot, J.-P. Lessard, and J.-C. Nave. Stationary non-radial localized patterns in the planar Swift-Hohenberg PDE: Constructive proofs of existence. *Journal of Differential Equations*, 414:555–608, 2025.
- [16] R. Calleja, C. Garcia-Azpeitia, O. Henot, J.-P. Lessard, and J. Mireles-James. From the Lagrange Triangle to the Figure Eight Choreography: Proof of Marchal’s Conjecture. [arXiv:2406.17564](https://arxiv.org/abs/2406.17564), 2024.
- [17] S. Day, J.-P. Lessard, and K. Mischaikow. Validated Continuation for Equilibria of PDEs. *SIAM Journal on Numerical Analysis*, 45(4):1398–1424, 2007.
- [18] J. Gallian. *Contemporary Abstract Algebra*, volume 10. Cengage, 2020.
- [19] M. Gameiro and J.-P. Lessard. Analytic estimates and rigorous continuation for equilibria of higher-dimensional PDEs. *Journal of Differential Equations*, 249(9):2237–2268, 2010.
- [20] M. Gameiro and J.-P. Lessard. Efficient rigorous numerics for higher-dimensional PDEs via one-dimensional estimates. *SIAM Journal on Numerical Analysis*, 51(4):2063–2087, 2013.
- [21] D. Hill, J. Bramburger, and D. Lloyd. Approximate localised dihedral patterns near a Turing instability. *Nonlinearity*, 36(5):2567–2630, 2023.
- [22] D. Hill, J. Bramburger, and D. Lloyd. Dihedral rings of patterns emerging from a Turing bifurcation. *Nonlinearity*, 37(3):035015, 2024.

- [23] O. Hénot. Radiipolynomial.jl, 2022. <https://github.com/OlivierHnt/RadiiPolynomial.jl>.
- [24] D. Lloyd and B. Sandstede. Localized radial solutions of the Swift-Hohenberg equation. *Nonlinearity*, 22(2):485–524, 2009.
- [25] D. J. Lloyd. Hexagon invasion fronts outside the homoclinic snaking region in the planar Swift-Hohenberg equation. *SIAM J. Appl. Dyn. Syst.*, 20(2):671–700, 2021.
- [26] D. J. B. Lloyd, B. Sandstede, D. Avitabile, and A. R. Champneys. Localized hexagon patterns of the planar Swift-Hohenberg equation. *SIAM J. Appl. Dyn. Syst.*, 7(3):1049–1100, 2008.
- [27] E. Makrides and B. Sandstede. Existence and stability of spatially localized patterns. *J. Differential Equations*, 266(2-3):1073–1120, 2019.
- [28] A. Mielke. Instability and stability of rolls in the Swift-Hohenberg equation. *Comm. Math. Phys.*, 189(3):829–853, 1997.
- [29] H. Sakaguchi and H. R. Brand. Stable localized squares in pattern-forming nonequilibrium systems. *Europhysics Letters*, 38(5):341, May 1997.
- [30] J. van den Berg, Jan Bouwe Williams. Rigorously Computing Symmetric Stationary States of the Ohta-Kawasaki Problem in Three Dimensions. *SIAM J. Math. Anal.*, 2019.
- [31] J. van den Berg, Jan Bouwe Williams. Optimal periodic structures with general space group symmetries in the Ohta-Kawasaki problem. *Physica D (Nonlinear Phenomena)*, 2021.
- [32] J. B. van den Berg, M. Breden, J.-P. Lessard, and M. Murray. Continuation of homoclinic orbits in the suspension bridge equation: A computer-assisted proof. *Journal of Differential Equations*, 264(5):3086–3130, 2018.
- [33] J. B. van den Berg, M. Breden, J.-P. Lessard, and L. van Veen. Spontaneous periodic orbits in the navier-stokes flow. *Journal of nonlinear science*, 31(2):1–64, 2021.
- [34] J. B. van den berg, O. Hénot, and J.-P. Lessard. Constructive proofs for localized radial solutions of semilinear elliptic systems on  $\mathbb{R}^d$ . *Nonlinearity*, 36(12):6476–6512, 2023.